

Revealing Local and Directional Aspects of Catalytic Active Sites by the Nuclear and Surface Electrostatic Potential

Joakim Halldin Stenlid^{1,2,#,*} and Frank Abild-Pedersen^{1,*}

¹ SUNCAT Center for Interface Science and Catalysis, SLAC National Accelerator Laboratory, 2575 Sandhill Road, Menlo Park, California, 94025, United States.

² SUNCAT Center for Interface Science and Catalysis, Department of Chemical Engineering, Stanford University, 443 Via Ortega, Stanford, California, 94305, United States.

[#] *Current address: KBR, Inc, Intelligent Systems Division, NASA Ames Research Center, Moffett Field, California 94035, United States*

** Email: joakim.halldin.stenlid@nasa.gov (JHS) and abild@slac.stanford.edu (FA-P)*

ABSTRACT (200 words): This work examines the prospects of using the electrostatic potential, $V(\mathbf{r})$, as descriptor in heterogeneous catalysis. In particular, the subatomic spatial resolution of the property allows for analysis of both directionality and confinement effects in surface adsorption. This feature of $V(\mathbf{r})$ is used to identify adsorption sites, orientations, and energetics for metal surfaces, particles, and nanoclusters upon interactions with catalytically relevant intermediates. The use of $V(\mathbf{r})$ in assessing the 3D nature of catalytic sites in low-temperature and electrocatalysis is highlighted, and future directions in catalysis design discussed. Ultimately, we provide a critical analysis of the use of $V(\mathbf{r})$ in predictions of local adsorption susceptibilities, and we address its limitations. The link between $V(\mathbf{r})$ and other established descriptors in catalysis are motivated via physical relations and theoretical derivations; close ties are established between $V(\mathbf{r})$ and the d -band center (ϵ_d), as well as the surface site stability (BE_M). By comparing the performance of $V(\mathbf{r})$ evaluated on isodensity contours, i.e., the surface electrostatic potential, to that of $V(\mathbf{r})$ evaluated at the nucleus of an atom, we investigate the application space for a directional and an atom-localized version of the $V(\mathbf{r})$ descriptor for catalyst design.

1. INTRODUCTION

In heterogeneous catalysis theory, surface adsorption energies are quintessential performance-governing properties of the catalytic material from which catalytic turnovers, reaction selectivity, and deactivation susceptibility can be derived.¹⁻⁷ Nevertheless, adsorption energies are not fundamental properties of the material but instead a mutual response to the perturbation that the surface site and adsorbate exerts on each other upon interaction; the adsorption response is, thus, dictated by more intrinsic properties of the material and adsorbate. Deriving a theoretical framework that predict adsorption behavior from fundamental materials properties simultaneously provides physical insight into catalytic activity while allowing for an accelerated estimation of the catalytic capacity of a material.^{1,6} Such physics-guided approaches have therefore been a successful pathway towards exploring the vast chemical space for in-silico design of catalytic materials with tailored characteristics.

The d -band model of Nørskov and co-workers is a prime example of the benefits of a model that takes fundamental properties as input in predictions of catalytic performance.^{8,9} Derived from Newns-Anderson theory^{10,11}, the d -band model links the Fermi level-referenced center of the metal d -states to the relative ability of a transition metal surface to form chemical bonds with an adsorbate. Thereby, adsorption trends can be rationalized over the periodic system, which has been

used extensively in catalyst design.^{8,9} For transition metal oxides and other ionic materials, the *d*-band model cannot be applied, however. Instead, efforts in creating a unified theory for adsorption has identified useful performance descriptors such as the O *p*-band center or bulk metal-oxide bond strengths obtainable from, e.g., the crystal orbital Hamiltonian population (COHP) analysis.^{12,13} There are, in fact, a multitude of fundamental materials properties that can, and has been, used as catalysis descriptors and that suits different classes of materials; examples include the cohesive energy, number of valence electrons, upper band edge of the *d*-band, electrostatic potential, ionization potential, electron affinity, polarizability, and structural properties such as lattice coordination number.^{14–23} While many of these properties have been successfully employed in data-driven and machine learning models,^{24–34} there is both scientific and practical value in exploring the physicochemical origin of catalytic activity through physics-derived models.^{19–21,35–45} In particular, we envisage that continued theory development toward capturing the three-dimensional (3D) spatial property distribution of a dynamic active site is a critical step to understand and design materials for low-temperature and electrocatalysis. The latter is essential in the strive towards sustainable industrial chemical transformation processes.

At this point, it is instructional to introduce the distinction between global and local materials descriptors. While global descriptors represent the entire material, a local descriptor only represents a distinct part of the material.⁴⁶ A benefit of a global descriptor is the comparably rapid and unambiguous evaluation of the property. The disadvantage is that surface interactions are local in nature and therefore varies with fluctuations in the local surface structure and composition. Capturing the locality of surface interactions becomes particularly important for structurally diverse systems (such as rough surfaces or surfaces that undergo dynamical restructuring), surfaces with a wide compositional distribution (such as alloys), or where intra- or intermolecular co-adsorbate effects has a large influence on the surface properties (e.g., through surface oxidation or for multidentate adsorption). Evaluating local descriptors comes with the challenge of accounting for perturbation⁴⁷ of the local properties of the active site by variations in the nearby environment; e.g., while local versions of the *d*- and *p*-band descriptors can be generated through site projected density of states (DOS),⁴⁸ one still needs to include additional properties such as the filling of *d*-states of the neighboring atoms to accurately account for compositional changes of an alloy and to capture the variation in adsorption energetics.^{49,50} The metal atom binding energy of a site is another example of a property that scales with adsorption energy and is sensitive to the local environment.^{21,36,38,51} These site-specific local scaling relations have been successfully exploited in the coordination-environment based alpha-parameter scheme,³⁶ generalized coordination number,²⁰ orbital-wise coordination number,¹⁹ and related approaches.^{18,52}

For multiple circumstances, however, not even atom-resolved locality is enough to fully capture the surface interaction. In cases where surface co-adsorbates or the surrounding medium such as an electrolyte also interacts with the adsorbate, the situation becomes exceedingly complex and oftentimes dynamic in nature. One can compare this situation – in which the adsorbate resides in a solvent pocket – to the field of enzymatic catalysis, where the active site is a three-dimensional (3D) adsorption pocket. In enzymes, the delicate interplay between amino acid moieties, cofactors, and metal centers dictates the mode of catalytic action. For this purpose, analyzing property distributions within the catalytic pocket is an attractive approach that can be applied also to

heterogeneous catalysis. For instance, the so-called molecular surface property approach (MSPA)⁵³ that utilizes properties such as the electrostatic potential as well as the local electron affinity and ionization potential mapped onto isodensity contours, have displayed promising results for predicting the magnitude and directionality of interactions between molecules as well as adsorption onto metal and oxides surfaces of nanoclusters, nanoparticles and extended surfaces.^{53–63}

This work focuses on employing the electrostatic potential as guide in heterogeneous catalysis applications. Examined material include transition metal compounds known to possess catalytic activity in many chemical reactions of industrial and academic relevance.^{6,7} The spatial variation of the electrostatic potential, $V(\mathbf{r})$, is computed using GGA-DFT. The position and magnitude of its local minima and maxima in $V(\mathbf{r})$ when mapped on isodensity contours are used to predict relative adsorption propensities and adsorption loci on metal surfaces, nanoparticles, and nanocluster. $V(\mathbf{r})$ has the advantage of being an intrinsic property of a chemical compound and a physical observable. In addition, $V(\mathbf{r})$ is rigorously defined within DFT and plays a well-supported role in the formation of chemical bonds, as demonstrated theoretically and in practice.^{64–68} An added trait is the relative ease of computing the $V(\mathbf{r})$ property that converges faster with the accuracy in the electronic structure compared to total energies, including, e.g., adsorption energies.⁶⁹ While the directionality of $V(\mathbf{r})$ makes it attractive, we also consider the nuclear electrostatic potential, $V_{0,A}$, as a descriptor, evaluated at the core of an atom. Doing so allows us to compare and connect the electrostatic potential to other well-established local descriptors in heterogeneous catalysis. $V_{0,A}$ has been used in the so-called Alchemical approach to predict adsorption energies onto isovalent metal compounds,^{70–72} within conceptual DFT to study surface chemistry of materials,^{73–83} and it has been used in the description of metal complex redox chemistry.⁸⁴ It can, furthermore, be theoretically shown that the nuclear electrostatic potential scale with the binding energy of atoms in chemical compounds.^{65,69,85–89} We use this information to explore the fundamental link between the electrostatic potential, the metal atom binding energies (BE_M), and the local d -band center (ϵ_d) of metal and metal alloy surfaces. The current work constitutes an early step towards accounting for the 3D (spatial) nature of an active site (*cf.* a 3D motif) and its near environment in catalysis. Future work will aim at exploring the 3D character of an active site in more detail. We envisage that the electrostatic potential will serve as a valuable fundamental property in this process providing guidance in active site design.

2. METHODS

Unless otherwise stated, all calculations have been carried out in the VASP 5.4.4 program suit^{90,91} using the RPBE⁹² flavor of GGA-DFT. We use the standard PAW core potentials^{93,94} and expand the valance states on 400 eV plane-wave basis-sets. The Brillouin zone was sampled on Γ -centered \mathbf{k} -meshes with a maximum \mathbf{k} -spacing of 0.3 \AA^{-1} (corresponding, e.g., to a $5 \times 5 \times 1$ k-mesh on a 2×2 surface supercell of a Cu fcc(100) surface facet) for the periodic surface and using the Γ -point only for nanoparticles and gas phase species. The lattice constants of the fcc metals were obtained from Roling et al.²¹ Surface models were generated using the atomic simulation environment (ASE).⁹⁵ A minimum vacuum distance between periodic images of at least 15 \AA was enforced for all structures. Symmetric slab structures were used where possible in evaluating the local descriptors.

When computing adsorption and binding energies, asymmetric slabs combined with dipole corrections were used. All electronic energies and forces where converge to 10^{-6} eV and 0.03 eV/Å, respectively. The ϵ_d values were evaluated using the VASPKIT software.⁹⁶

The electrostatic potential, $V(\mathbf{r})$, was outputted directly from VASP without the exchange-correlation potential (i.e., using LVHAR = .TRUE.) following the below formula

$$V(\mathbf{r}) = \underbrace{\sum_A \frac{Z_A}{|\mathbf{R}_A - \mathbf{r}|}}_{\text{nuclei}} - \underbrace{\int \frac{\rho(\mathbf{r}') d\mathbf{r}'}{|\mathbf{r}' - \mathbf{r}|}}_{\text{electrons}} \quad (1)$$

In the above, Z_A and \mathbf{R}_A refer to the charge and position of the nucleus A , while \mathbf{r} and $\rho(\mathbf{r})$ correspond to the spatial coordinate and the electronic density function, respectively. $V(\mathbf{r})$ was mapped onto 0.001 a.u. (atomic units) isodensity contours with the local maxima and minima analyzed and visualized with the VESTA software.⁹⁷ The 0.001 a.u. isodensity contour correspond closely to typical interaction distances of non-covalent interactions.^{65,98} The minima and maxima in the surface electrostatic potential are referred to as $V_{S,\min}$ and $V_{S,\max}$, respectively (also known as σ -lumps and σ -holes⁵⁸). The electrostatic core potentials, $V_{0,A}$, were also outputted directly from VASP as the average of a small but finite spherical volume at the core determined by the ENAUG tag (here set to 587 eV corresponding to the default value of Cu with the largest value in the fcc metals series). $V_{0,A}$ of nuclei A is given by

$$V_{0,A} = \sum_{B \neq A} \frac{Z_B}{|\mathbf{R}_B - \mathbf{R}_A|} - \int \frac{\rho(\mathbf{r}) d\mathbf{r}}{|\mathbf{r} - \mathbf{R}_A|} \quad (2)$$

where B is an index of all atoms of the compound with $B \neq A$. As alluded to in the introduction, the $V(\mathbf{r})$ property converges fast relative to other electronic structure-based properties (such as energetics and electronic band structure) with regards to the accuracy of the computational settings.⁶⁹ In **Note S1**, we demonstrate that the descriptor quality is maintained for different DFT xc-functionals (spanning LDA to meta-GGA), varied PAW potentials, plane-wave basis set with cut-offs as small as 174 eV, as well as for vacuum distances down to 5 Å (if using internal, but not an external, reference for the absolute vacuum potential in the latter case). In general, the electrostatic potentials obtained by VASP (or any other 3D periodic code), are arbitrarily shifted with respect to the absolute scale. For comparison between different compounds, the potential must be shifted to the same scale. The shift can be achieved by relating the potential to a reference, either an external (typically using the plateau value of the potential in the vacuum region) or an internal (e.g., the core potential of a bulk atom), see **Note S5**.

All structures and adsorption/binding energies obtained in this study are uploaded to the Catalysis Hub database,⁹⁹ and can be accessed directly via <https://www.catalysis-hub.org/publications/StenlidRevealing2024>.

3. RESULTS AND DISCUSSION

In the following, the prospect of employing the electrostatic potential, $V(\mathbf{r})$, as descriptor in heterogeneous catalysis is critically explored, while also identifying certain shortcomings. The text is organized with an initial comparison between the directional (spatial) and local character of $V(\mathbf{r})$ when mapped onto isodensity contours, known as the surface electrostatic potential, $V_S(\mathbf{r})$. This will be followed by a discussion where the local, atom-specific features of $V(\mathbf{r})$ are compared, and theoretically linked, to other well-established descriptors in heterogeneous catalysis based on fundamental materials properties. **Table S1** summarizes the comparison of surface chemisorption descriptors used in this work. Finally, an outlook is provided on the incorporation of $V(\mathbf{r})$ in evaluation of the 3D character of an active site via a discussion on the influence of co-adsorbates.

a. Locality and directionality of the surface electrostatic potential

As an introduction to the concepts, adsorption tendencies onto metal nanoparticles and nanoclusters are investigated. The first example comes from Roling et al. who mapped out the adsorption of CO onto a series of TM_{147} cuboctahedral fcc transition metal (TM) nanoparticles (**Figure 1.A**). The atom-resolved susceptibility to adsorption in the ontop mode was linked to the local site stability determined as the binding energy (BE_M) of the metal to its site. Excellent prediction of the adsorption preferences onto the corner, edge, as well as the (100) and (111) terrace ontop sites was demonstrated as reproduced in **Figure 1.B**. BE_M is an example of a local descriptor, which in this case provides a single estimate (one descriptor value) per surface atom. BE_M is an attractive descriptor as it can be evaluated from structural features without the need for additional DFT calculations. However, BE_M is non-directional since it does not contain information about the orientation of the interaction.

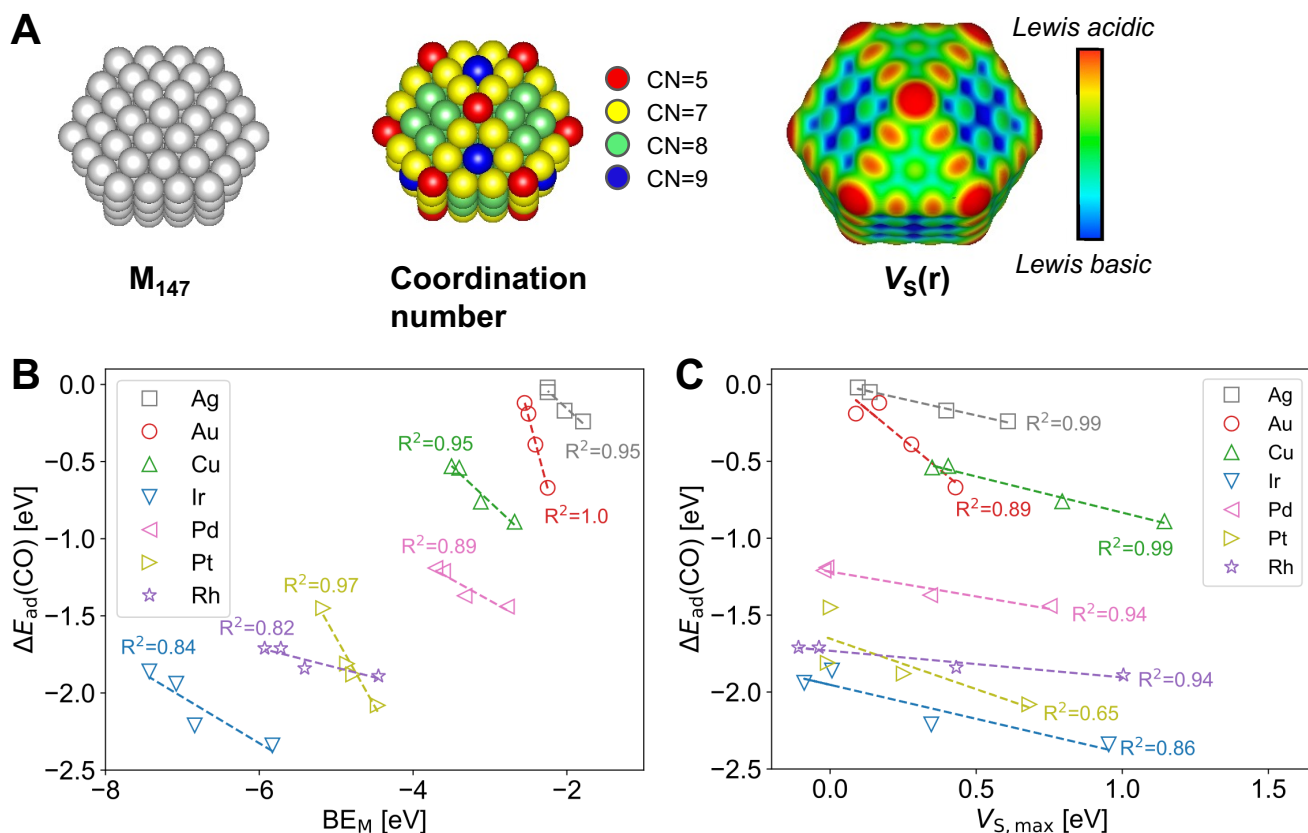


Figure 1. Adsorption energy predictions for cuboctahedral TM_{147} nanoparticles. In **A**, cuboctahedral TM_{147} NP with local coordination number depicted and $V_s(\mathbf{r})$ map shown at the 0.001 a.u. isodensity surface. **B** and **C** shows the trends for CO adsorption onto the unique surface sites of the TM NPs versus site stability (BE_M) and maxima in $V_s(\mathbf{r})$ ($V_{S,max}$). Mean absolute errors (MAEs) in eV for **B**: Ag = 0.02, Au = 0.01, Cu = 0.03, Ir = 0.07, Pd = 0.03, Pt = 0.04, Rh = 0.03; **C**: Ag = 0.01, Au = 0.06, Cu = 0.02, Ir = 0.07, Pd = 0.02, Pt = 0.01, Rh = 0.02. The BE_M and CO ΔE_{ad} data was obtained from Roling et al.¹⁰⁰

A similar analysis of TM_{147} nanoparticles can be provided using $V(\mathbf{r})$ as descriptor, as we have shown for Au, Cu, and Pt particles in our previous work.^{55,56} In brief, when evaluated on an isodensity surface contour, the surface electrostatic potential, $V_s(\mathbf{r})$ provides information about regions of the chemical compound with local electron (i.e., negative charge) accumulation or depletion with regards to the arrangement of the atomic nuclei.^{53,65} This generates local maxima, $V_{S,max}$, and local minima, $V_{S,min}$, on the isodensity surface (**Figure 1.A**). Because the repulsive contribution of electron overlap is approximately constant on the isodensity surface, the variation of the $V_s(\mathbf{r})$ property indicates interaction tendencies of the compound (assuming for now that other interaction modes such as charge-transfer and polarization are negligible). We here note that the number of local $V_{S,max}$ and/or $V_{S,min}$ of a certain atom can, and often do, differ from unity and hence more than one unique adsorption site can be identified for the same atom.^{53,57} This fact will be discussed in further detail in connection to nanoclusters later in the text. For non-covalent interactions, such as a hydrogen- or halogen-bonds,^{101–103} electrostatic forces largely govern the interplay between two compounds, with charge-transfer and polarizability as a higher-order correction factors. In such circumstances, $V_{S,max}$ and $V_{S,min}$ thus identifies electron accepting and

donating sites, respectively, on a compound, which often correlates with Lewis acidity/basicity (electrophilicity/nucleophilicity).⁵³ The compound could, e.g., be a catalyst surface, an adsorbate, or an electrolyte molecule. The direction of the interaction will be controlled by the location of the local extreme values in $V_S(\mathbf{r})$,^{53,65} which, in principle, should be matched with the $V_S(\mathbf{r})$ distribution of the interacting compound.^{53,59}

For interactions involving significant rehybridization of the electronic states, it is not obvious that $V_S(\mathbf{r})$ will control the interaction. In addition, there have been reports suggesting that the electrostatic potential is not well defined for compounds with degenerate or near-degenerate ground states such as metals as well as metal particles and clusters.^{104,105} Correlations have, nonetheless, been shown between maxima/minima ($V_{S,\max}/V_{S,\min}$) and adsorption energies in several instances, including the adsorption of CO on transition metal nanoclusters, nanoparticles, and surfaces.^{53,55–59,61} For these compounds, the position and magnitude of $V_{S,\max}$ on the substrate provides predictions about the position and strength of the CO atop adsorption, with $V_{S,\max}$ attracting the negative lone-pair region of the C-end of CO. **Figure 1.C** includes the correlation between the $V_{S,\max}$ descriptor and the CO adsorption energies onto the TM₁₄₇ nanoparticles of Roling et al.¹⁰⁰ It is clear that the predictive power is on-par with that of the BE_M descriptor. Two interesting details from **Figure 1.C** pertain to the slope of the Au correlation that deviate significantly from the slope of the other metals, and the surprisingly (from the perspective of the $V_{S,\max}$ predictions) weak adsorption energy of CO on Pt(111) that leads to a comparatively large scatter in the Pt trend. Intriguingly, the results also suggest that there is a connection between $V(\mathbf{r})$ and the TM BE_M, as shown in **Figure S2**. In addition, $V_S(\mathbf{r})$ retains its predictive ability when computed with numerous different functionals and (inaccurate to accurate) computational settings as shown in **Figure S1**.

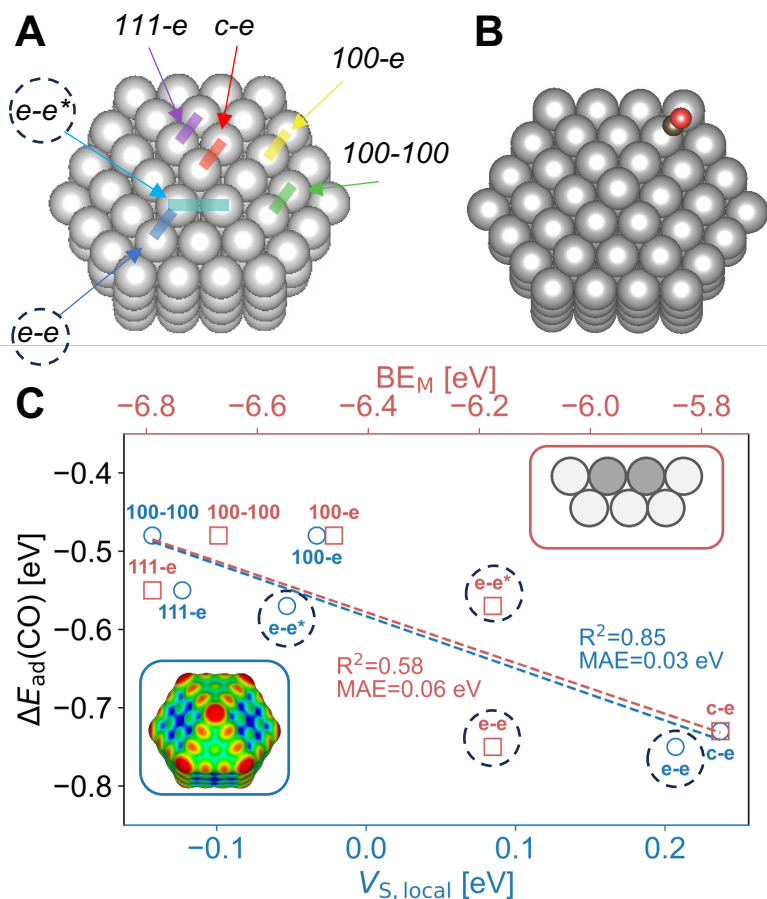


Figure 2. Directional adsorption at edge and bridge sites of cuboctahedral Cu_{147} NP. All unique bridge adsorption positions are depicted in **A**. **B** displays the favored adsorption orientation of CO at the e-e edge site. In **C**, correlation plot between the adsorption energy (ΔE_{ad}) of CO (obtained from Roling et al.¹⁰⁰) as a function of the local $V_S(\mathbf{r})$ value at the saddle point of the bridge sites ($V_{S,\text{local}}$) and as function of the average metal binding energy of the site (BE_M) as obtained from the alpha parameter scheme of Roling et al.²¹

We now turn our attention to two situations where the directionality of $V(\mathbf{r})$ can provide additional insights not available with a local but non-directional descriptor such as BE_M or ϵ_d (see **Figure 2.A**): i) multiple adsorption sites at the same atom; ii) adsorption sites at different atoms that only become distinct when the unique directionality of adsorption is accounted for.

As example of i) above, we use ontop edge sites on TM_{147} . Here one possible adsorption position is with the adsorbate pointing straight out from the edge having approximately 120° angles with respect to the two flanking terraces. Alternative positions are with the adsorbate directed perpendicular to either of the (100) or (111) terraces. **Figure 2.B** shows the preferred ontop adsorption position of CO at the edge of the Pt_{147} particle. This is correctly identified as the one with $\sim 120^\circ$ angles versus the terraces from the position of the $V_{S,\text{max}}$. Attempting to adsorb CO perpendicular to either terrace leads to the barrierless convergence to the favored site. For this example, using a non-directional descriptor would not have allowed us to predict the adsorption position and angle.

As example of ii), we use adsorption to bridge sites. On a TM_{147} particle, there is a step-edge bridge site located in-between two atoms that both have coordination number 7 (i.e., bridge site 7-7, denoted $e-e$ in **Figure 2.A**). However, there is also a 7-7 bridge site spanning over the corner of the (111) terrace from one edge to another (denoted $e-e'$ in **Figure 2.A**). These two 7-7 sites will be assigned the same descriptor value if using a non-directional descriptor, such as BE_M (when estimated using average single site BE_M values). **Figure 2.C** compares the predicted trend in adsorption energies of CO onto bridge sites of Cu_{147} particle using the BE_M and $V_S(\mathbf{r})$ descriptors. $V_S(\mathbf{r})$ is evaluated at the saddle point (local minima) at the bridge sites. One can see that the predictions are similar between BE_M and $V_S(\mathbf{r})$ except for the 7-7 sites; while BE_M predicts the same adsorption energy, $V_S(\mathbf{r})$ correctly ranks the 7-7 edge site (the $e-e$ site) as having a stronger adsorption susceptibility compared to the 7-7 corner site ($e-e'$ site). This tendency is likely related to the location of the adsorption site at a tilted angle with respect to the (111) terrace for the 7-7 edge site, which makes adsorption more favorable compared to adsorption to the 7-7 terrace site.

The positional and orientational analysis of the edge sites translates to extended surfaces. Comparing edges of the (211) facet for different fcc metals, the location of the $V_{S,\text{max}}$ over the ontop edge sites shifts (**Figure 3.A**). There is a distinct difference here between the coinage metals (Cu, Ag, Au) compared to the metals (Pt, Ir, Pd, Rh); whereas the coinage metals have $V_{S,\text{max}}$ located at a tilted angle polarized over the terrace, the other metals display $V_{S,\text{max}}$ straight above the atom with respect to the subsurface atoms. This is in fact well in line with previous results for metal nanoclusters where the location of $V_{S,\text{max}}$ (or σ -holes as they are known as in the MSPA community⁵³) is explained in terms of electron depletion resulting from the formation of σ -bonds between the metal atoms.⁵⁷ Because the σ -holes of coinage metals are the result of s -orbital interactions (since the d -states are filled), the resulting σ -hole is diffuse and a combined effect of all (local) metal-metal interactions. For non-coinage metals, the σ -holes are of mixed d - and s -orbital origin with the directionality of the d -orbitals often dominating the position of the σ -hole (i.e., $V_{S,\text{max}}$) and masking the influence of the s -states. The orbital analysis explains the position of the $V_{S,\text{max}}$ on the (211) fcc surfaces, with $V_{S,\text{max}}$ located at the tangent of subsurface-surface bonds for non-coinage metal surface and diffused at an angle with respect to the extension of the surface-subsurface bond for coinage metals.

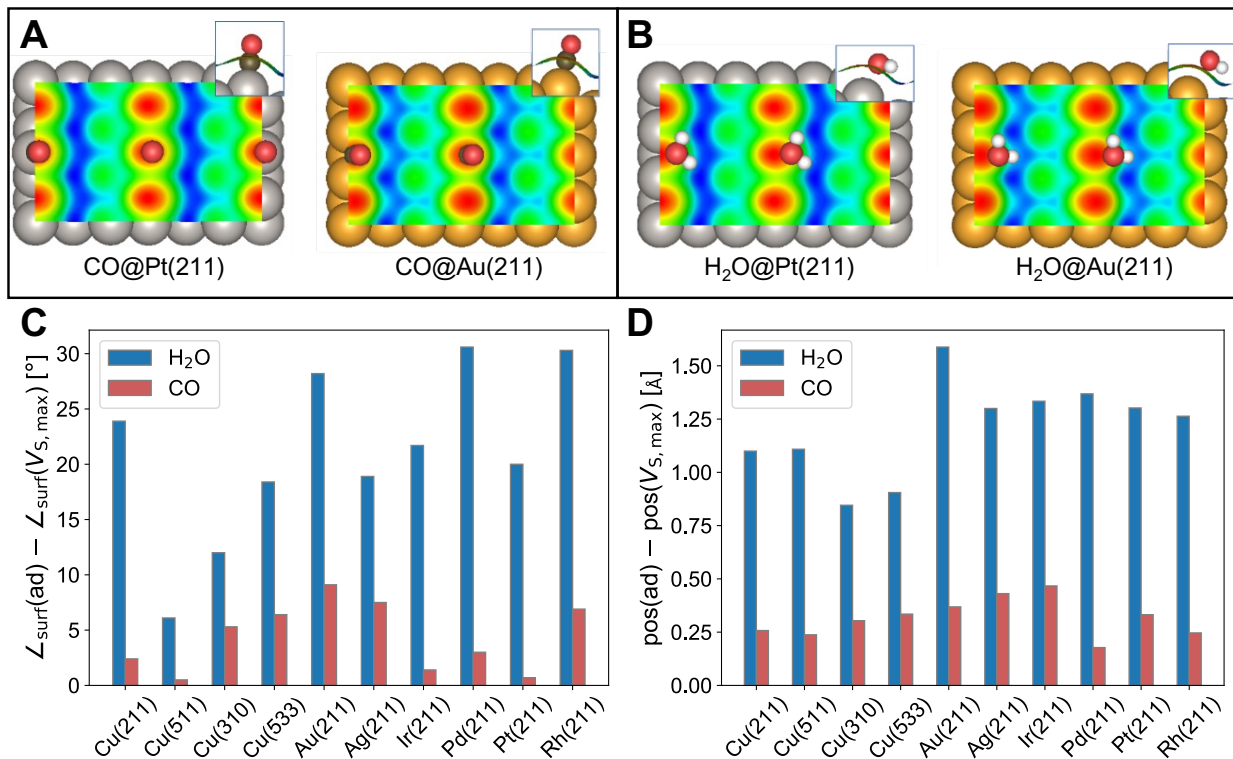


Figure 3. Adsorption tendencies onto TM step edge surfaces. In **A** and **B**, $V_s(\mathbf{r})$ mapped onto the 0.001 a.u. isodensity contour of Pt(211) and Au(211) surfaces, with adsorption position of CO and H₂O in **A** and **B**, respectively. The adsorption angle (\angle_{surf}) with respect to the surface plane compared to the \angle_{surf} of the $V_{S,\text{max}}$ locus is shown in **C**, whereas the distance between $V_{S,\text{max}}$ and adsorbate the adsorption position (defined by coordinates of C and O for CO and H₂O, respectively) is included in **D**. Note that the 0.001 a.u. isodensity contour for which $V_{S,\text{max}}$ has been evaluated is often located at an elevation that is 0.1 to 0.2 Å shifted compared to the adsorption which adds a constant bias to the results in **D**.

The above directionality aspects affect the position of adsorbates at the edge site. Using, once again, CO as probe molecule, the angle at which it adsorbs to the (211) edge correlates closely with the angle of the $V_{S,\text{max}}$ (**Figure 3.A**). CO prefers to adsorb up-right on the non-coinage metals, but at an angle leaning over the surface terrace for Cu, Ag, and Au. **Figure 3.C** and **D** summarize the adsorption trends for different stepped surfaces in terms of adsorption angle and adsorption position relative to the $V_{S,\text{max}}$. The analysis highlights that other non-(211) stepped surfaces facets of coinage metals also adsorb CO at an angle, again correlating with $V_{S,\text{max}}$ as visualized in **Figure S3** for Cu(310), (511), and (533). These facets represent different types of steps flanked by different combinations of (100) and (111) terraces at varied step separation. Examining the H₂O adsorbate provides some instructional insights. When H₂O adsorbs O-down at the edge, it is torn between interacting at the favored position for M-O bonding and leaning out over the terrace to form a H-bond to the surface; beneath the step, the surfaces display an area with accumulated electron density leading to a significant $V_{S,\text{min}}$ (also known as a σ -lump⁵³) towards which H is attracted. Whether or not H₂O is distorted from the edge site depends on the location of the $V_{S,\text{max}}$ at the edge, the magnitude of the interactions, as well as the distance between the sites set by the lattice parameter of the metal as well as by the crystal orientation of the facet and in part by the

directionality of the $V_{S,\max}$. We find that H_2O tends to stay at the edge site for the non-coinage metals but forms H-bonds with the surface for the coinage metals at a position that best compromises between H-bonds and M-O bonds, see **Figure 3.C**. Hence, the directionality of surface properties again plays a critical role in dictating surface interactions.

As a final example of directionality, we discuss metal nanoclusters. Nanoclusters are small particles with properties largely dominated by quantum-size effects. In our previous work, we have looked into nanoclusters of TM in vacuum, and their interactions with both electrophilic and nucleophilic adsorbates.^{55,57,58,61} An interesting feature of nanoclusters is the distinction between their different σ -holes depending on the filling of the d -states.⁵⁷ For Pt-group clusters, in particular, the $V_S(\mathbf{r})$ profiles give rise to a large number of unique $V_{S,\max}$, oftentimes multiple sites per atom. **Figure 4.A** shows the example of Pt_{13} from Stenlid et al.⁵⁷ Despite its C_2 symmetry, $V_{S,\max}$ identifies several unique positions exceeding the number of atoms in the Pt_{13} particle. Pt nanoclusters are particularly important in catalysis applications, for instance in emission control of CO, NO_x and CH_4 .^{106,107} In addition, it is known that the Pt nanoclusters can exist in various configurations due to the small energy difference between different shapes and the fluxionality of the particles.^{108–113} Hence, sampling all possible surface interactions is challenging but necessary to capture the catalytic behavior of Pt nanoclusters. Such a challenge can be aided using proper descriptors. In this direction, we place the abovementioned Pt_{13} cluster on the common catalysis support of CeO_2 .¹¹⁴ Upon adhesion to the surface support, the particle retains multiple distinct σ -holes albeit (**Figure 4.B**). We find that the σ -holes identify adsorption sites well and that CO adsorbs preferentially at the positions of the $V_{S,\max}$ (**Figure 4.C**). On the other hand, the magnitude of the $V_{S,\max}$ correlates poorly with the adsorption energy to the site suggesting that additional factors dominate the strength of interaction. This is in agreement with previous results for the Pt_{13} cluster when interacting with Lewis bases such as H_2O ,^{57,61} and it follows the general conclusions of Lamoureux et al.¹¹⁵ that small TM nanoparticles and clusters exhibit complex interaction relationships. The complexity seems to simplify for coinage metal nanoclusters, however; we have shown in previous work that the $V_S(\mathbf{r})$ descriptor is able to predict interaction patterns and rank site preferences on nanoclusters of Au, Ag and Cu.^{55,57,58} In addition, interactions with Lewis acids onto Pt nanoclusters have displayed good correlations between $V_{S,\min}$ and adsorption energies.⁶¹ $V_S(\mathbf{r})$ profiles thus provide a valuable tool for analysis of adsorption onto TM nanoclusters, with a necessity to include additional information in order to capture adsorption trends onto non-coinage metal clusters.

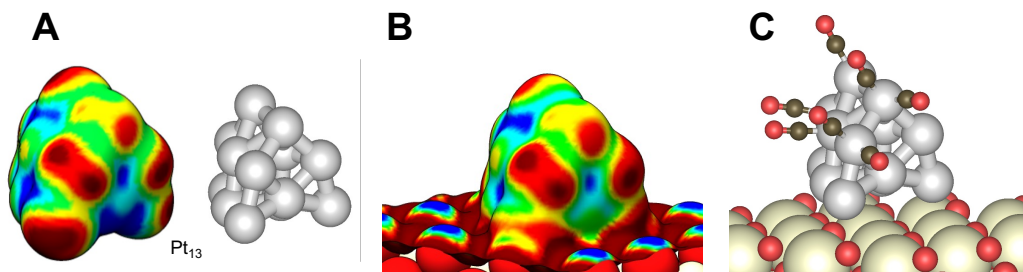


Figure 4. Adsorption propensity of a supported Pt_{13} nanocluster. In **A**, the vacuum $V_S(\mathbf{r})$ of Pt_{13} is mapped at the 0.001 a.u. isodensity contour. Note the C_2 symmetry of the nanocluster. **B** shows the same

cluster adsorbed at the CeO₂(111) surface. **C** depicts superimposed adsorption structures of CO at the different adsorption positions identified by $V_{S,max}$ (the CO molecules are not adsorbed simultaneously). Figure **A** is readapted from Stenlid et al.⁵⁷ under the terms of the CC BY 4.0 license (<https://creativecommons.org/licenses/by/4.0/>). Copyright 2017, The Authors, Published by MDPI, Basel, Switzerland.

All in all, the above analysis demonstrates the benefits of using a directional descriptor for analysis of interaction tendencies in metal-based catalysis. The $V(\mathbf{r})$ descriptor can localize interaction sites on monometallic transition metal clusters, particles, and surfaces. While capturing interaction trends on non-coinage nanoclusters is sometimes elusive to $V(\mathbf{r})$, $V_{S,max}$ correlates well with adsorption energies onto larger TM particles and surfaces, as well as coinage metal nanoclusters. In the following sections, we shall explore the use of $V(\mathbf{r})$ when comparing the catalytic behavior of different metal and metal alloy surfaces, as well as the connection of $V(\mathbf{r})$ to other well-established reactivity descriptors.

b. Physical relation of $V(\mathbf{r})$ to descriptors in heterogeneous catalysis

In this section, we explore the physical rationale behind the use of $V(\mathbf{r})$ as descriptor for adsorption to heterogeneous catalyst surfaces, and we investigate its ability to predict adsorption behavior when comparing different compounds. For non-covalent interactions (i.e., physisorption), the connection between adsorption energies and the distribution in the electrostatic potential is motivated by fundamental physics; if the adsorbate can be described as a point charge and the substrate is non-polarizable, the local electrostatic potential gives the exact interaction energy. Electrostatic effects remain of central importance also when the interaction leads to a perturbation of the interacting compounds such as polarization and rehybridization of electronic states.^{65,85} Nevertheless, the question why information about $V(\mathbf{r})$ at the ground state of the substrate provides information about surface-adsorbate chemisorption deserves a deeper analysis.

To address the question above, we introduce the nuclear electrostatic potential (also known as the core potential), $V_{0,A}$ described by eq. 2. This is a singular property, specific to each unique atom in a compound. $V_{0,A}$ summarizes the chemical environment of the atom similar to a chemical shift in x-ray photoemission spectroscopy (XPS) or nuclear magnetic resonance (NMR) spectroscopy.^{69,85,87} First, a few empirical observations are made; **Figure 5.A** shows that there is a close correlation between $V_{0,A}$ of the surface atoms and the identified $V_{S,max}$ of the TM₁₄₇ nanoparticles discussed in the previous section (*cf.* **Figure 1**). Consequently, the close correlation between $V_{S,max}$ and the BE_M of the site as well as with adsorption energy of CO also holds for $V_{0,A}$ (**Figure 5.B-C**). These relations are useful in understanding the role of the electrostatic potential in chemisorption.

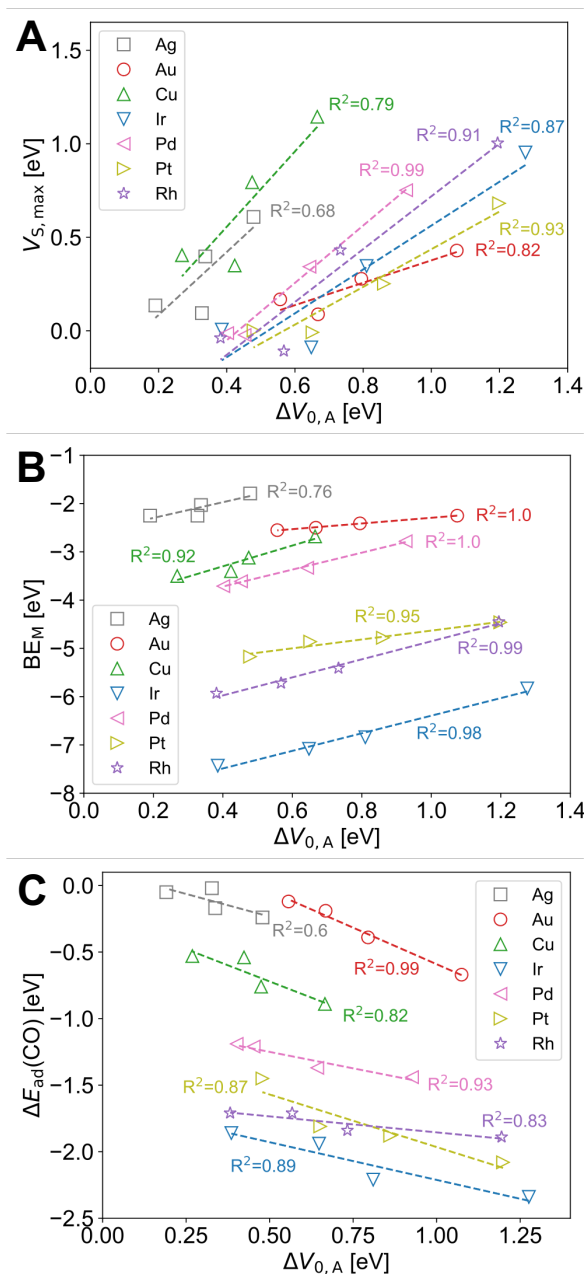


Figure 5. Correlation plots nuclear electrostatic potential for TM_{147} NPs. $V_{0,A}$ at unique surface sites of cuboctahedral TM_{147} nanoparticles versus the site-specific $V_{S,max}$ (in **A**), BE_M (**B**), and CO ΔE_{ad} (**C**), respectively. Mean absolute errors (MAEs) in eV, **A**: Ag = 0.10, Au = 0.04, Cu = 0.13, Ir = 0.12, Pd = 0.03, Pt = 0.07, Rh = 0.11; **B**: Ag = 0.08, Au = 0.05, Cu = 0.08, Ir = 0.07, Pd = 0.02, Pt = 0.05, Rh = 0.06; **C**: Ag = 0.05, Au = 0.02, Cu = 0.05, Ir = 0.05, Pd = 0.02, Pt = 0.07, Rh = 0.03. The BE_M and CO ΔE_{ad} data was obtained from Roling et al.¹⁰⁰

The correlation between $V_{0,A}$ and BE_M shown in **Figure 5** is particularly interesting. Starting from the Newns-Anderson model for surface chemisorption, one can derive a relation between adsorption energies and the local cohesive energy of a site (i.e., BE_M).⁵⁰ This relation has

also been inferred experimentally.^{116,117} Similarly, the physical relationship between the ε_d (or, more exact, the upper d -band edge) and BE_M has been theoretically derived and demonstrated via DFT calculations.⁴⁹ As alluded to in the introduction, the ε_d (upper d -band edge for early TM) is closely linked to adsorption energies and a well-established descriptor of catalysis.^{8,9} The link between the electrostatic potential and the BE_M and ε_d properties can be further rationalized. It has been known since Wilson’s seminal work¹¹⁸ that there exists a physical relation between the nuclear electrostatic potential and the energy of an atom by interaction over the sequential addition of its Z electrons via:

$$E_{atom} = \int_{Z'=0}^Z (V_0 Z')_N dZ' \quad (\text{eq. 3})$$

This relation was extended to molecules by Politzer and Parr as:⁸⁶

$$E_{mol} = \sum_A Z_A \int_{\lambda=0}^1 (V_0(\lambda))_N d\lambda \quad (\text{eq. 4})$$

The relation between $V_{0,A}$ and the molecular energy (E_{mol}) was later demonstrated computationally yielding a linear relation between E_{mol} and the sum of $V_{0,A}$ of all atoms A.⁶⁹ This suggests, that there is a link between $V_{0,A}$ and the energy of an atom in a chemical compound. While the relation is most accurate for small atoms, the relationships provide a rationale for the connection between $V_{0,A}$ and BE_M found in this work. It also serves as further motivation for the use of $V(\mathbf{r})$ as a descriptor for surface interactions and in catalysis applications.

c. Nuclear and surface $V(\mathbf{r})$ for molecular adsorption energy predictions on fcc metals

Under operation, catalytic surfaces display a large variety of active sites. The surface will expose a plethora of step, kink, corner, and terraces sites, all with different coordination environment and, oftentimes, varied catalytic activity. The $V_S(\mathbf{r})$ and $V_{0,A}$ properties changes with the local environment of the surface, as shown in **Figure 6** and **Figure S4** for a series of fcc surfaces. These include the (100), the (111), and the stepped (211) facets, where atoms are added incrementally until a full new monolayer is created. $V_S(\mathbf{r})$ and $V_{0,A}$ are compared to DFT-computed adsorption energies for the OH, CO, and CH₃ adsorbates at the ontop sites of these surfaces as reported by Roling et al.¹⁰⁰ BE_M for the metal atoms onto these sites were also reported, which can be regarded as another adsorbate. The variations in $V_S(\mathbf{r})$ and $V_{0,A}$ are used to predict adsorption energies onto the abovementioned surfaces and $V_S(\mathbf{r})$ as well as $V_{0,A}$ as shown in **Figure 7**. **Figure 7.A-B** includes a summary of the total predictions spanning all surfaces and adsorbates, while **7.C-K** show a selection of cases (Ir, Pt, and Au; OH and CH₃ adsorbates) with detailed information in **Note S3**. **Figure S5-S8** and **S10-S12** contain the full data series. The correlations are overall strong, with MAE within 0.2 eV for each series and below 0.1 eV overall, but with certain challenges as discussed in the next paragraph. The results also corroborates the close relationship between BE_M of the metal sites and the computed $V_S(\mathbf{r})$ and $V_{0,A}$ properties (see **Figure S9** and **S13**). Both $V_S(\mathbf{r})$ and $V_{0,A}$ are good descriptors of local adsorption tendencies with $V_{S,\max}$ yielding slightly enhanced predictions compared to $V_{0,A}$, which is reasonable owing to the more nuanced information provided by the surface electrostatic potential.

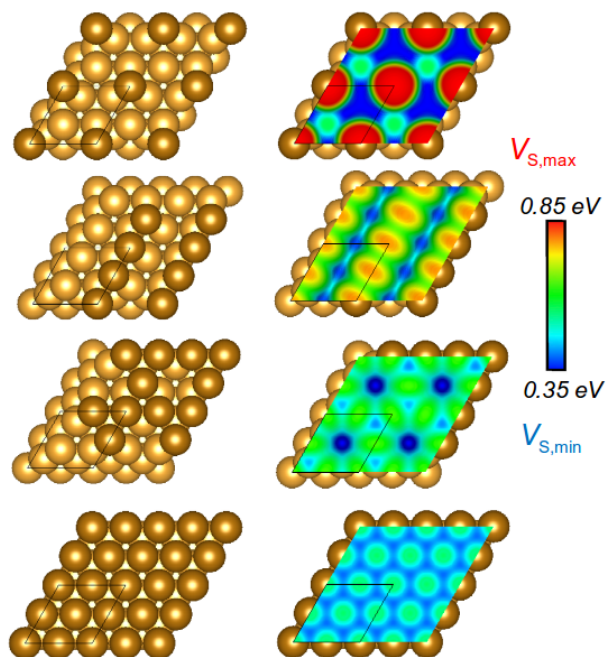


Figure 6. $V_S(\mathbf{r})$ maps on metal surfaces with adatoms. Results for the Cu(111) facet at the 0.001 a.u. isodensity surface. A comparison of the $V_S(\mathbf{r})$ maps for other facets is contained in **Figure S4**.

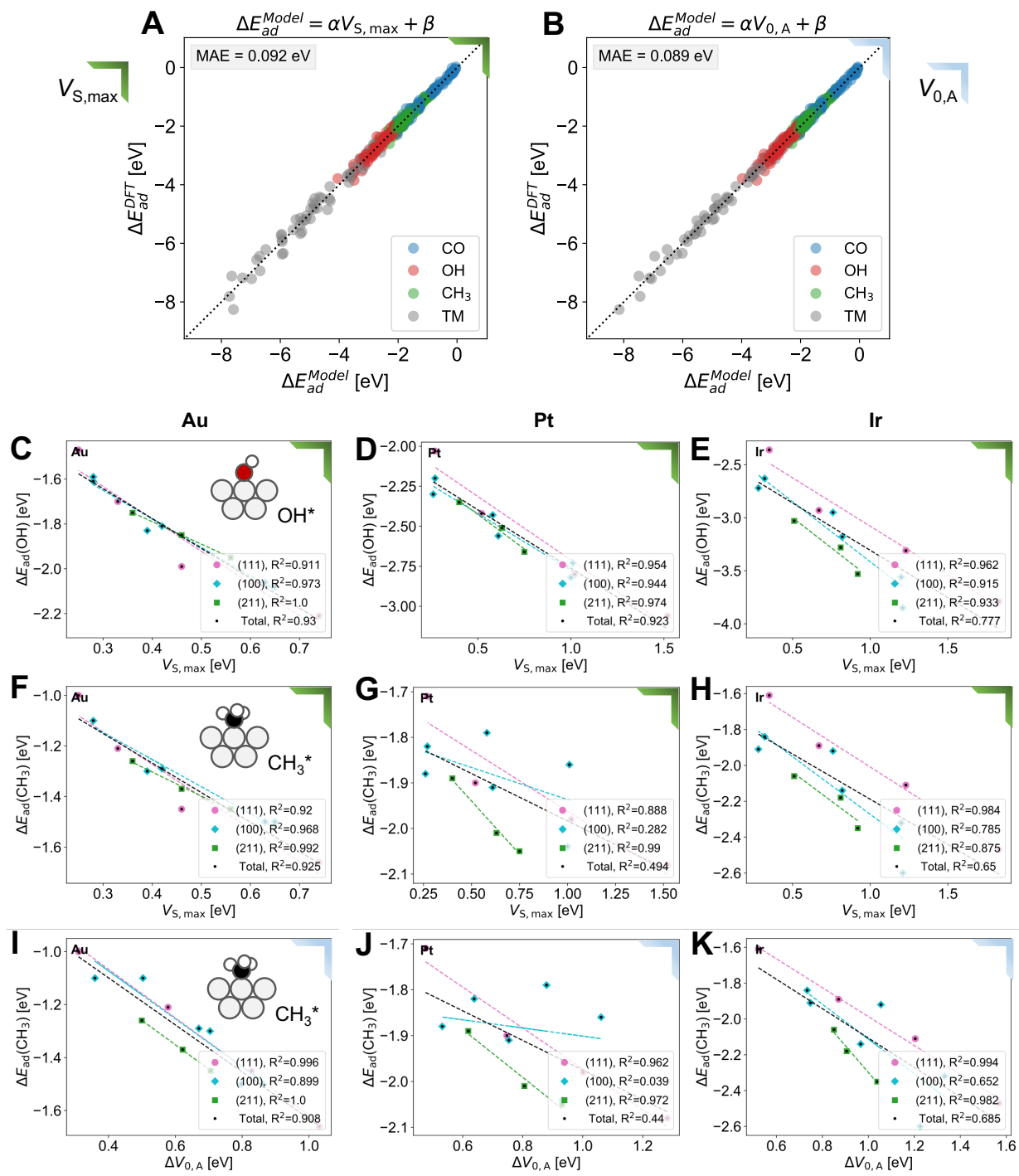


Figure 7. Correlation plots adsorption energies versus $V(r)$. In A and B, estimated adsorption energies for TM(211) surfaces with TM={Au, Ag, Cu, Ir, Pd, Pt, Rh} and the TM, CO, CH₃, OH adsorbates using $V_{S,max}$ and $V_{0,A}$ as descriptors, respectively. Detailed results for surfaces and adsorbates are included in Figure S5-S13. The BE_M and ΔE_{ad} data was obtained from Roling et al.¹⁰⁰

By now, it is not surprising that the predictions made by $V_S(\mathbf{r})$ and $V_{0,A}$ are of similar quality as those of BE_M as a result of the linear relation between $V(\mathbf{r})$ and BE_M . Consequently, the $V(\mathbf{r})$ descriptors perform well on the cases where BE_M excels and is less accurate for cases challenging to BE_M . In general, the coinage metals show strong correlation between $V(\mathbf{r})$ and adsorption energies, whereas the non-coinage metals result in larger scatter. The latter can be compared to the difficulty in ranking adsorption energies onto nanoclusters of non-coinage metals, whereas adsorption trends for coinage metal nanoclusters can be closely reproduced (see discussion in previous section). Comparing different adsorbates, CO yields strong correlation with coinage metals but almost no correlation on the Pd, Pt, Ir, and Rh surfaces. In contrast, CH_3 and OH show quite strong correlations with BE_M as well as $V(\mathbf{r})$ on most surface. Relating back to the original work of Roling et al.,¹⁰⁰ where the weak correlations for certain cases were tied to the effect the adsorbate induced on the stability of the adsorption site as measured by the slope between the BE_{M-ads} vs BE_M . A stronger influence yields a slope, k , smaller than one, whereas a weak influence results in a slope close to one. The relation between E_{ads} and BE_M is $1-k$. Hence, a weak influence on the stability of the metal site of an adsorbate will result in weak correlation between BE_M and the adsorption energy, which will translate directly to the results for $V(\mathbf{r})$. As an example, CO have a weak influence on the BE_M of the non-coinage metals, but a clear influence on the coinage metals, rationalizing the observed correlations.

A similar analysis can be performed using the average electron attachment energy, $E_S(\mathbf{r})$, as descriptor (see **Note S4**).^{53,56,62} This property contains information about the band structure in addition to the electrostatic potential. Consequently, it provides information about charge-transfer/polarization ability of the surface site. If such factors would be influential (and orthogonal to $V(\mathbf{r})$) in determining the adsorption energies, it is expected that $E_S(\mathbf{r})$ should provide improved estimates of interaction trends.⁵⁸ As the estimates of $E_S(\mathbf{r})$ are closely tracing those of $V_S(\mathbf{r})$ (**Figure S15-S17**), the conclusion is that accounting for charge-transfer/polarization is not essential for the studied systems.

Dissecting the interaction trends for adsorption onto extended surfaces in more detail, we break down adsorption energy prediction into the contributions of different facets. It becomes evident that the predictions are more accurate within a given facet than for the whole metal dataset (**Figure 7** and **Figure S5-13**). The observation is true for both the $V(\mathbf{r})$ descriptors, as well as BE_M . One can, however, also note that the correlations between BE_M and $V(\mathbf{r})$ is facet-dependent (**Figure S9** and **S13**). Hence, there could be a noteworthy effect unaccounted for when comparing the different facets precluding assessment on an equal footing. A part of the reason for the separate trends of the facets lies in the choice of reference. Determining $V(\mathbf{r})$ for a 3D periodic system, the relative scale for $V(\mathbf{r})$ is shifted by a constant and needs to be corrected by relating it to a known reference. Often, an external reference is used by taking the average electrostatic potential in vacuum as reference corresponding to $V(\mathbf{r}) = 0$. The data presented above is analyzed using an external reference. However, equally valid is employing an internal reference such as the nuclear electrostatic potential of a bulk atom. The latter approach is often the choice in band alignment calculations. **Figure 8.A** shows a comparison between the correlation between BE_M for a number of surface sites on Cu facets and $V_{0,A}$ computed with the external vacuum reference versus using the internal bulk nuclear potential in each calculation. The Cu facets comprise (100), (110), (111),

(211), (310), (511) as well as (533), and include a wide variety of terrace and step sites. It is evident from **Figure 8.A** that using the internal reference is beneficial. This result partly explains the strong facet-dependence in the surface results. While minor improvements in the trends for the external reference approach can be obtained by employing larger vacuum distances, larger basis sets cutoffs and denser \mathbf{k} -point sampling (see **Note S5** and **Figure S18**), the complete understanding of the effect of the choice of reference will be the topic of a future work.

One exciting opportunity to utilize $V(\mathbf{r})$ is in estimations of the local BE_M for arbitrary metals structures, such as rough surfaces.¹¹⁹ We test the predicative power of the linear trend for the data with using the internal reference in **Figure 8.A** for a previously unseen Cu surface, Cu(643). **Figure 8.B.** indicate good predictions with a MAE of ~ 0.10 eV. This is promising for another area of application related to accelerated training of model parameters. The BE_M descriptor can, e.g., be estimated through a wealth of methods including coordination-based approaches, semi-empirical relationships, and machine learning. The α -parameter scheme of Abild-Pedersen and coworkers provides a fast way of predicting BE_M based on parameters representing each bond between atoms in the compound. Typically, parameters for an elemental fcc metal are trained against 14 DFT calculations of BE_M values for various surface structures. Using calibrated $V(\mathbf{r})$ relations, the number of DFT calculations can be significantly reduced. **Figure S19** shows in detail the approach and results, highlighting that the number of calculations can be cut from 14 to 6 by using a small Cu_{147} calibration nanoparticle, and a larger nanoparticle representing a wide range of surface sites.

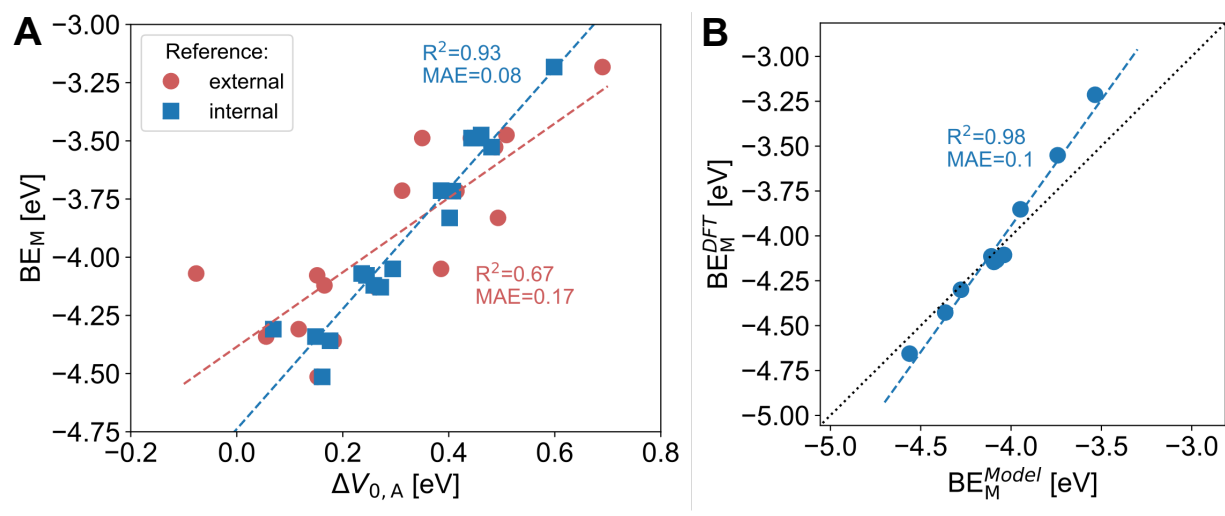


Figure 8. $V_{0,A}$ adsorption predictions on Cu hkl facets. In **A**, correlations between $V_{0,A}$ and BE_M for all unique adsorption sites on Cu(hkl) surfaces using external (vacuum) and internal (bulk atom) reference electrostatic potentials, respectively, for (hkl) = (100), (110), (111), (211), (310), (511), and (533). In **B**, the correlation in **A** for the internal reference is used to predict the BE_M on an unseen surface, Cu(643).

d. Alloys and the relation between $V(r)$, BE_M and ϵ_d

Alloys are an important class of compounds that offer catalytic properties not available in monometallic systems. In particular, the wealth of unique surface motifs that can be created for multimetallic compounds comprising varied composition and coordination environments expose a wide engineering space for designing catalytic active sites with tailored properties.^{120,121} Traversing this vast chemical space is, however, a daunting endeavor that can be greatly aided using descriptor-based high-throughput methods.

Among the many descriptors evaluated for alloys, both the ϵ_d (or the upper d -band edge) as well as the BE_M descriptors have been extensively used.^{6,18–20,48,51,52,119} There are well-known challenges,^{8,122} which in large parts can be rationalized by a second-order perturbation to the adsorption energy from the filling of the d -states of the neighboring atoms of the adsorption site – an effect not captured by the ϵ_d nor fully by the BE_M .⁵⁰ As BE_M is an adsorption property itself, it is also affected by the second-order perturbation of the neighboring atoms which leads to a weakened correlation between BE_M and the ϵ_d . Another manifestation of the second-order effect is that BE_M follow separate scaling relations for variation in compositional and structural space.^{36,50} In the following, we shall investigate how $V(r)$ is affected by alloying.

Figure 9.A shows the variation in $V_{0,A}$ of the Au surface atoms for near surface alloys of Au(111) with the second layer fully alloyed with $5d$ TMs sweeping from La to Au. The variations are compared to variations in the adsorption energy of atomic oxygen, $E_{\text{ads}}(\text{O})$, from Saini et al.,⁵⁰ and contrasted to the variations in BE_M . A similar plot is included in Saini et al.⁵⁰ for the variation in $E_{\text{ads}}(\text{O})$ and ϵ_d . All quantities follow a parabolic variation with the filling, f_d , of the d -states of the alloying atom (**Figure 9.A** and **Figure S20**). However, the parabolic behavior is most pronounced for $E_{\text{ads}}(\text{O})$ and BE_M , and weakest for the ϵ_d and $V_{0,A}$. The data reveals a linear relation between the variation in $V_{0,A}$ and the ϵ_d , whereas the $V_{0,A}$ and BE_M data forms what appears to be a periodic relationship (**Figure 9.B**). For mid- to late transition metals (W to Pt), there is a linear relation between $V_{0,A}$ and BE_M , while for the early transition metals and coinage metals, the linearity is broken. This traces the behavior of ϵ_d versus $E_{\text{ads}}(\text{O})$ from Saini et al.⁵⁰ and has two origins; one is the second order effect from the d -filling of the neighboring atoms alluded to in the above discussion which originates in the expected variation in the local cohesive energy with alloying (see Hammer et al.⁹); another is the role of the upper-edge of the d -band, which for non-coinage metals is the main factor correlating with the availability of bonding and antibonding states upon adsorption.⁴⁹ The ϵ_d correlates with the latter until the d -states of the adsorption site are pushed so low in energy that the d -band width no longer can compensate. To avoid detachment from the Fermi-level and a disrupted correlation between the quantities is observed. Due to the close relation between $V_{0,A}$ and the ϵ_d for the complete set of studied data, one can apply a corresponding rationale on the behavior of $V_{0,A}$ with BE_M as the filling of the alloying atoms are varied. Ultimately, the result is that $V_{0,A}$ can be used as descriptor for adsorption energies replacing the ϵ_d , and with second order corrections needed to capture trends over the periodic table. When compared, the BE_M descriptor displays a fairly good correlation with the $E_{\text{ads}}(\text{O})$ over the series of NSA, **Figure 9.C**. In contrast, $V_{0,A}$, display a close linear relationship with $E_{\text{ads}}(\text{O})$ only for the alloys containing late TMs, **Figure 9.D**.

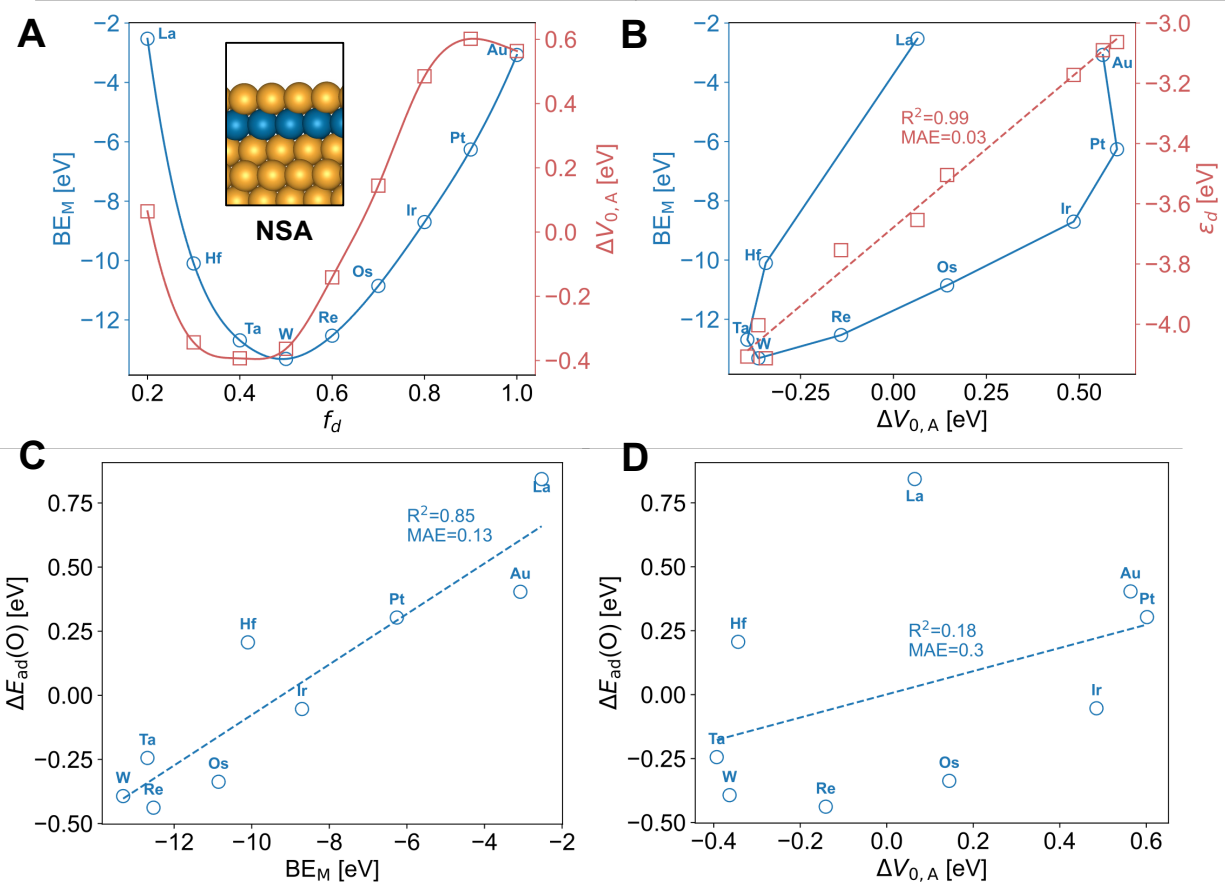


Figure 9. Descriptors for adsorption energies onto near surface alloys. Correlations plots between varied surface properties on near surface alloys (NSAs) of Au(111) with a subsurface layer of 5d TMs. The ϵ_d and $\Delta E_{ad}(O)$ data was obtained from Saini et al.⁵⁰

To corroborate the discussion above, we create a series of surface alloys for Cu(100) with late transition metals (Au, Ag, Pt, Pd, Ir, Rh). The degree of alloying around a surface Cu site is varied from zero to four neighbors (0-100%) as shown in **Figure 10.A**. Because the series comprises only late transition metals, linear relationships between $V_{0,A}$, and BE_M as well as the ϵ_d are expected. The $V_{0,A}$, and BE_M as well as the ϵ_d properties all varies linearly with the degree of alloying, as shown in **Figure S21**. There are also linear relations between the properties $V_{0,A}$, and BE_M as well as the ϵ_d , in particular within each a given Cu-TM alloy series with the same element (**Figure 10.B-C**). Interestingly, while most of the TM series yield similar slopes and intercepts, there are a few exceptions. For instance, whereas most metals display a more negative core potential with weaker BE_M , Ir display the opposite trend. A similar relation is found for $V_{0,A}$ versus the ϵ_d . Additional details are enclosed in **Note S7**. The effect of these findings on prediction of adsorption energies and catalytic activity, will be the topic of future studies.

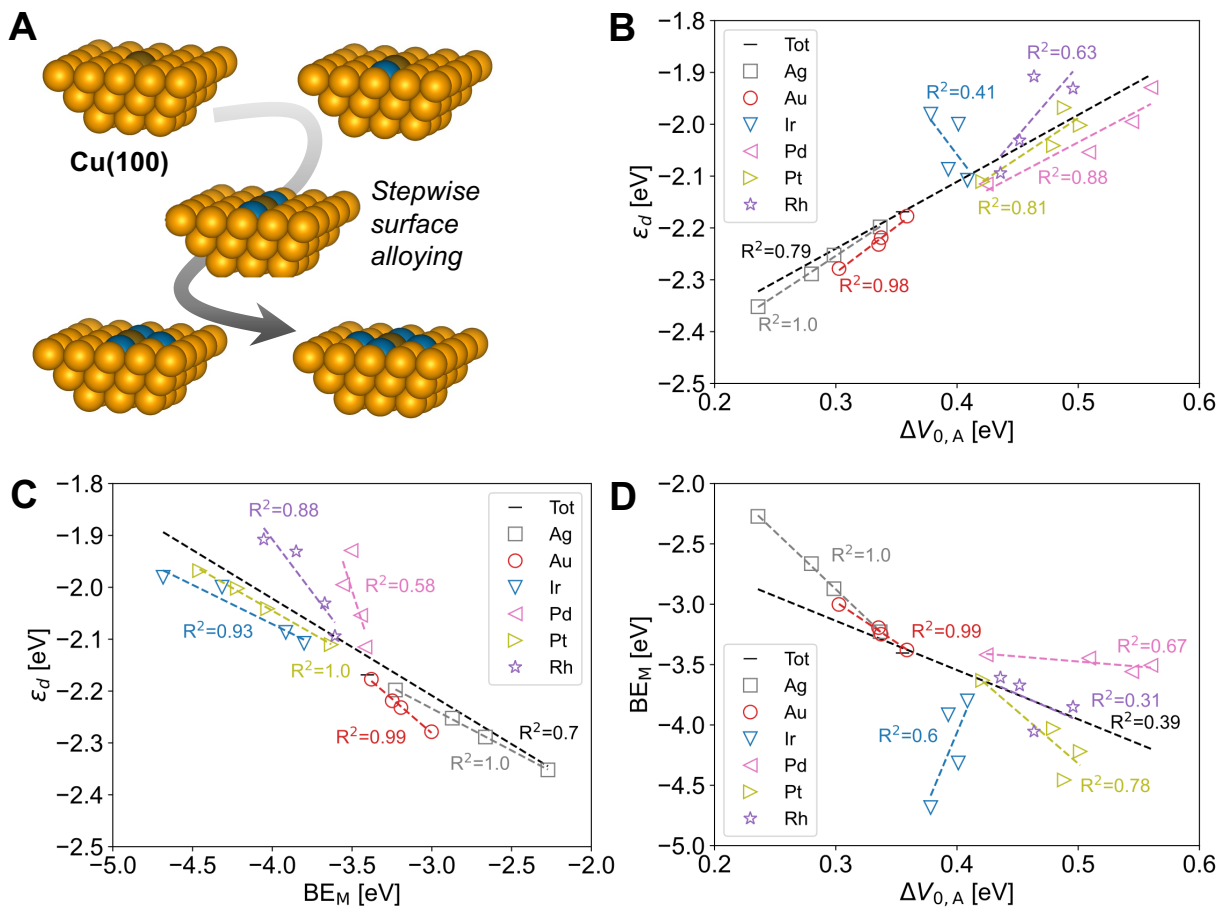


Figure 10. Adsorption and property trends for Cu surface alloys. In **A**, schematic of surface alloying for Cu(100) with $TM = \{Au, Ag, Ir, Pd, Pt, Rh\}$. The Cu ontop adsorption site is highlighted with a darker shade of brown and the alloying TM colored blue. In **B**, correlation between the surface properties $V_{0,A}$, and BE_M as well as ϵ_d .

e. Co-adsorption and outlook

As an outlook towards possible future applications of $V_S(\mathbf{r})$ in assessing the 3D nature of low temperature and electrochemical active sites in heterogeneous catalysis, we return to the topic of directionality. Co-adsorption is considered a crucial factor in low temperature catalysis, where it can shift the adsorption energies by several eV. The co-adsorbates can be duplicates of the interacting species itself, or other active or inactive species. By tuning the influence of co-adsorbates, catalytic performance can be promoted or inhibited.¹²³

We create a model systems of a Pt(111) surface where varied first row atomic adsorbates. B, C, N, O, and F are placed in the fcc sites surrounding an ontop adsorption site as depicted in **Figure 11.A**. These adsorbates have different influence on the ontop site. Via through-bond effects, the adsorbates modulate the susceptibility of the ontop site to interactions as demonstrated

by the variations in the local $V_{S,\max}$, **Figure 11.B**. The co-adsorbates will also influence adsorption via through-space effects, where the electrostatic potential of the adsorbate interacts with dipoles of the adsorbate. Of the series of co-adsorbates, B yields a positive electrostatic potential whereas $F \approx O > N > C$ result in negative local electrostatic potentials. We use H_2O as probe molecule since it provides both Lewis acidic (H) and Lewis basic (O) ends. H_2O adsorbs O-down towards the Pt atop site and can rotate freely to form non-covalent bonds with the adsorbate, or to minimize repulsion. The inserts in **Figure 11.C** shows the favored orientation for H_2O with differently charged co-adsorbates. For negatively charged co-adsorbates, H_2O orients to maximize H-donation to the adsorbates. For B (positively charges), H_2O detaches from the surface and orients its negative lone pairs towards the co-adsorbate. The adsorption energy of H_2O scales with the magnitude of $V_S(\mathbf{r})$ ($V_{S,\max}$ for B, $V_{S,\min}$ for the remaining co-adsorbates) of the co-adsorbate, **Figure 11.C**, but also with the magnitude of $V_{S,\max}$ at the adsorption site, **Figure S22**.

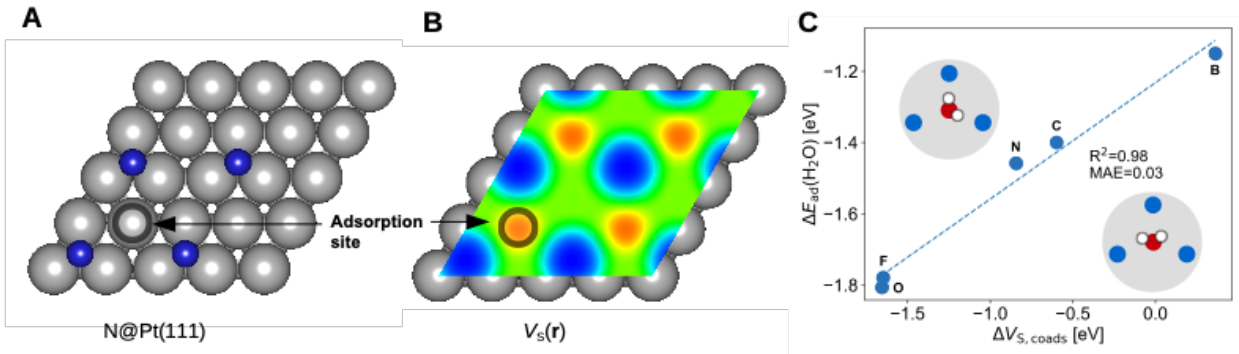


Figure 11. Coadsorption effects on adsorption energies. In A, a 0.25 ML N^* decorated Pt(111) surface, and in B, the corresponding $V_S(\mathbf{r})$ mapped at the 0.001 a.u. isodensity contour. By varying the coadsorbate, H_2O adsorption onto an atop site correlates with the local electrostatic potential at the coadsorbate= $\{F, O, N, C, B\}$.

The results above hold promise for future applications of $V_S(\mathbf{r})$ in evaluation of the catalytic pockets (3D motifs) of low-temperature and electrocatalytic systems. Future work will explore these aspects in more detail. Despite the benefits of $V(\mathbf{r})$, we acknowledge that $V_S(\mathbf{r})$ is not a universal descriptor but will be best practiced in conjugation with complementary analysis using properties that capture other aspects of chemical interactions. For example, the second order effect of neighboring atoms d -filling on the electronic structure of the adsorption site will be needed to capture interactions on alloys. In this paper, we have discussed the close tie of $V(\mathbf{r})$ to the descriptors ϵ_d and BE_M , and the opportunities and limitations that $V(\mathbf{r})$ thus inherent. The added value of $V(\mathbf{r})$ with respect to these descriptors is the directionality of $V(\mathbf{r})$ lacking in many other local descriptors. Whereas $V(\mathbf{r})$ can be computed more rapidly than, e.g., adsorption energies, one clear shortcoming is the need to carry out expensive DFT calculations, while a descriptor such as BE_M that is based on analytic relationships can be computed essentially instantaneously.

4. CONCLUSION

This study has delved into the utilization of the electrostatic potential, $V(\mathbf{r})$, leveraging in particular its spatial properties, as a guide in heterogeneous catalysis applications. The assessment of $V(\mathbf{r})$ through GGA-DFT computations, with a focus on its local minima and maxima

mapped on isodensity contours, proves a valuable instrument in predicting relative adsorption propensities and determining adsorption loci on metal surfaces, nanoparticles, and nanoclusters. The intrinsic nature of $V(\mathbf{r})$ as a material property that is a physically observable quantity and rigorously defined within DFT, enhances its significance. The directionality of $V(\mathbf{r})$ allows for subatomic understanding of the features governing catalytic capacity of active sites. This is of particular importance to low temperature and electrochemical heterogeneous catalysis where co-adsorbates and the surrounding media play crucial parts.¹²⁴ Additionally, the use of the nuclear electrostatic potential, $V_{0,A}$, evaluated at the core of an atom, provides a comparative framework with well-established local descriptors in heterogeneous catalysis. The theoretical correlation between $V_{0,A}$ and atom binding energies in chemical compounds further strengthens its role as descriptor of surface reactivity. This work represents an initial stride towards comprehending the 3D spatial nature of an active site and its surroundings in catalysis. Future studies will delve deeper into the 3D characterization of active sites, with the expectation that the electrostatic potential will continue to serve as a fundamental property guiding catalyst design including both the active surface and its environment.

ACKNOWLEDGMENT

This research was supported by the U.S. Department of Energy, Office of Science, Office of Basic Energy Sciences, Chemical Sciences, Geosciences, and Biosciences Division, Catalysis Science Program to the SUNCAT Center for Interface Science and Catalysis. J.H.S. gratefully acknowledges financial support from the Knut and Alice Wallenberg Foundation (Grant No. 2019.0586). We acknowledge computational support from the National Energy Research Scientific Computing Center (Project Allocation No. m2997), a Department of Energy Office of Science User Facility supported by the Office of Science of the U.S. Department of Energy under Contract No. DE-AC02-05CH11231.

ASSOCIATED CONTENT

Supporting information:

Sensitivity test of computational settings; additional computational results including correlations between adsorption energies and local electrostatic potential; fitted parameters for the α -scheme; comparison of reference state for the electrostatic potential; description of and results for the electron attachment energy; summary of advantages and disadvantages of surface chemisorption descriptors.

AUTHOR INFORMATION

Corresponding authors

Joakim Halldin Stenlid, joakim.halldin.stenlid@nasa.gov

Frank Abild-Pedersen, abild@slac.stanford.edu

Author contributions

The authors jointly conceived the initial idea and designed the project. J.H.S performed the DFT calculations. The manuscript was written through the contributions of all authors. All authors have given approval to the final version of the manuscript

Funding

This research was supported by the U.S. Department of Energy, Office of Science, Office of Basic Energy Sciences, Chemical Sciences, Geosciences, and Biosciences Division, Catalysis Science Program to the SUNCAT Center for Interface Science and Catalysis. J.H.S. gratefully acknowledges financial support from the Knut and Alice Wallenberg Foundation (Grant No. 2019.0586).

Notes

The authors declare no financial conflict of interest

REFERENCES

- (1) Nørskov, J. K.; Bligaard, T.; Rossmeisl, J.; Christensen, C. H. Towards the Computational Design of Solid Catalysts. *Nat. Chem.* **2009**, *1*, 37–46.
- (2) Medford, A. J.; Vojvodic, A.; Hummelshøj, J. S.; Voss, J.; Abild-Pedersen, F.; Studt, F.; Bligaard, T.; Nilsson, A.; Nørskov, J. K. From the Sabatier Principle to a Predictive Theory of Transition-Metal Heterogeneous Catalysis. *J. Catal.* **2015**, *328*, 36–42..
- (3) Hoffmann, R. A Chemical and Theoretical Way to Look at Bonding on Surfaces. *Rev. Mod. Phys.* **1988**, *60*, 601–628.
- (4) Bligaard, T.; Nørskov, J. K.; Dahl, S.; Matthiesen, J.; Christensen, C. H.; Sehested, J. The Brønsted–Evans–Polanyi Relation and the Volcano Curve in Heterogeneous Catalysis. *J. Catal.* **2004**, *224*, 206–217.
- (5) Hammer, B.; Nørskov, J. K. Theoretical Surface Science and Catalysis—Calculations and Concepts. *Adv. Catal.* **2000**, *45*, 71–129.
- (6) Nørskov, J. K.; Studt, F.; Abild-Pedersen, F.; Bligaard, T. *Fundamental Concepts in Heterogeneous Catalysis*; John Wiley & Sons, 2014.
- (7) Schlögl, R. Heterogeneous Catalysis. *Angew. Chem. Int. Ed.* **2015**, *54*, 3465–3520.
- (8) Hammer, B.; Nørskov, J. K. Why Gold Is the Noblest of All the Metals. *Nature* **1995**, *376*, 238–240.
- (9) Hammer, B.; Nørskov, J. K. Theory of Adsorption and Surface Reactions. In *Chemisorption and Reactivity on Supported Clusters and Thin Films: Towards an Understanding of Microscopic Processes in Catalysis*; Lambert, R. M., Pacchioni, G., Eds.; 1997; pp 285–351.
- (10) Newns, D. M. Self-Consistent Model of Hydrogen Chemisorption. *Phys. Rev.* **1969**, *178*, 1123–1135.
- (11) Anderson, P. W. Localized Magnetic States in Metals. *Phys. Rev.* **1961**, *124*, 41–53.
- (12) Dickens, C. F.; Montoya, J. H.; Kulkarni, A. R.; Bajdich, M.; Nørskov, J. K. An Electronic Structure Descriptor for Oxygen Reactivity at Metal and Metal-Oxide Surfaces. *Surf. Sci.* **2019**, *681*, 122–129..
- (13) Comer, B. M.; Li, J.; Abild-Pedersen, F.; Bajdich, M.; Winther, K. T. Unraveling Electronic Trends in O* and OH* Surface Adsorption in the MO₂ Transition-Metal Oxide Series. *J. Phys. Chem. C* **2022**, *126*, 7903–7909.

- (14) Honkala, K. Tailoring Oxide Properties: An Impact on Adsorption Characteristics of Molecules and Metals. *Surf. Sci. Rep.* **2014**, *69*, 366–388.
- (15) Engel, J.; Schwartz, E.; Catlow, C. R. A.; Roldan, A. The Influence of Oxygen Vacancy and Ce³⁺ Ion Positions on the Properties of Small Gold Clusters Supported on CeO_{2-x}(111). *J. Mater. Chem. A* **2020**, *8*, 15695–15705.
- (16) Rahm, M.; Zeng, T.; Hoffmann, R. Electronegativity Seen as the Ground-State Average Valence Electron Binding Energy. *J. Am. Chem. Soc.* **2019**, *141*, 342–351.
- (17) Geerlings, P.; Chamorro, E.; Chattaraj, P. K.; De Proft, F.; Gázquez, J. L.; Liu, S.; Morell, C.; Toro-Labbé, A.; Vela, A.; Ayers, P. Conceptual Density Functional Theory: Status, Prospects, Issues. *Theor. Chem. Acc.* **2020**, *139*, 36.
- (18) Gao, W.; Chen, Y.; Li, B.; Liu, S.-P.; Liu, X.; Jiang, Q. Determining the Adsorption Energies of Small Molecules with the Intrinsic Properties of Adsorbates and Substrates. *Nat. Commun.* **2020**, *11*, 1196.
- (19) Ma, X.; Xin, H. Orbitalwise Coordination Number for Predicting Adsorption Properties of Metal Nanocatalysts. *Phys. Rev. Lett.* **2017**, *118*, 036101.
- (20) Calle-Vallejo, F.; Martínez, J. I.; García-Lastra, J. M.; Sautet, P.; Loffreda, D. Fast Prediction of Adsorption Properties for Platinum Nanocatalysts with Generalized Coordination Numbers. *Angew. Chem. Int. Ed.* **2014**, *53*, 8316–8319.
- (21) Roling, L. T.; Li, L.; Abild-Pedersen, F. Configurational Energies of Nanoparticles Based on Metal–Metal Coordination. *J. Phys. Chem. C* **2017**, *121*, 23002–23010.
- (22) Calatayud, M.; Markovits, A.; Menetrey, M.; Mguig, B.; Minot, C. Adsorption on Perfect and Reduced Surfaces of Metal Oxides. *Catal. Today* **2003**, *85*, 125–143.
- (23) Fuentealba, P.; Cárdenas, C. Density Functional Theory of Chemical Reactivity. In *Chemical Modelling: Volume 11*; Springborg, M., Joswig, J.-O., Eds.; The Royal Society of Chemistry, 2014; Vol. 11, pp 151–174.
- (24) Liu, X.; Cai, C.; Zhao, W.; Peng, H.-J.; Wang, T. Machine Learning-Assisted Screening of Stepped Alloy Surfaces for C₁ Catalysis. *ACS Catal.* **2022**, *12*, 4252–4260.
- (25) Pablo-García, S.; Morandi, S.; Vargas-Hernández, R. A.; Jorner, K.; Ivković, Ž.; López, N.; Aspuru-Guzik, A. Fast Evaluation of the Adsorption Energy of Organic Molecules on Metals via Graph Neural Networks. *Nat. Comput. Sci.* **2023**, *3*, 433–442.
- (26) Esterhuizen, J. A.; Goldsmith, B. R.; Linic, S. Uncovering Electronic and Geometric Descriptors of Chemical Activity for Metal Alloys and Oxides Using Unsupervised Machine Learning. *Chem Catalysis* **2021**, *1*, 923–940.
- (27) Mamun, O.; Winther, K. T.; Boes, J. R.; Bligaard, T. A Bayesian Framework for Adsorption Energy Prediction on Bimetallic Alloy Catalysts. *npj Comput Mater* **2020**, *6*, 1–11.
- (28) Ma, X.; Li, Z.; Achenie, L. E. K.; Xin, H. Machine-Learning-Augmented Chemisorption Model for CO₂ Electroreduction Catalyst Screening. *J. Phys. Chem. Lett.* **2015**, *6*, 3528–3533.
- (29) Jinnouchi, R.; Asahi, R. Predicting Catalytic Activity of Nanoparticles by a DFT-Aided Machine-Learning Algorithm. *J. Phys. Chem. Lett.* **2017**, *8*, 4279–4283.
- (30) Li, Z.; Wang, S.; Xin, H. Toward Artificial Intelligence in Catalysis. *Nat. Catal.* **2018**, *1*, 641–642.
- (31) Palizhati, A.; Zhong, W.; Tran, K.; Back, S.; Ulissi, Z. W. Toward Predicting Intermetallics Surface Properties with High-Throughput DFT and Convolutional Neural Networks. *J. Chem. Inf. Model.* **2019**, *59*, 4742–4749.
- (32) Chanussot, L.; Das, A.; Goyal, S.; Lavril, T.; Shuaibi, M.; Riviere, M.; Tran, K.; Heras-Domingo, J.; Ho, C.; Hu, W.; et al. Open Catalyst 2020 (OC20) Dataset and Community Challenges. *ACS Catal.* **2021**, *11*, 6059–6072.
- (33) Goeltl, F.; Mavrikakis, M. Generalized Brønsted-Evans-Polanyi Relationships for Reactions on Metal Surfaces from Machine Learning. *ChemCatChem* **2022**, e202201108.

- (34) Andersen, M.; Reuter, K. Adsorption Enthalpies for Catalysis Modeling through Machine-Learned Descriptors. *Acc. Chem. Res.* **2021**, *54*, 2741–2749.
- (35) Roling, L. T.; Abild-Pedersen, F. Structure-Sensitive Scaling Relations: Adsorption Energies from Surface Site Stability. *ChemCatChem* **2018**, *10*, 1643–1650.
- (36) Choksi, T. S.; Roling, L. T.; Streibel, V.; Abild-Pedersen, F. Predicting Adsorption Properties of Catalytic Descriptors on Bimetallic Nanoalloys with Site-Specific Precision. *J. Phys. Chem. Lett.* **2019**, *10*, 1852–1859.
- (37) Roling, L. T.; Choksi, T. S.; Abild-Pedersen, F. A Coordination-Based Model for Transition Metal Alloy Nanoparticles. *Nanoscale* **2019**, *11*, 4438–4452.
- (38) Dean, J.; Taylor, M. G.; Mpourmpakis, G. Unfolding Adsorption on Metal Nanoparticles: Connecting Stability with Catalysis. *Sci. Adv.* **2019**, *5*, eaax5101.
- (39) Streibel, V.; Choksi, T. S.; Abild-Pedersen, F. Predicting Metal–Metal Interactions. I. The Influence of Strain on Nanoparticle and Metal Adlayer Stabilities. *J. Chem. Phys.* **2020**, *152*, 094701.
- (40) Choksi, T. S.; Streibel, V.; Abild-Pedersen, F. Predicting Metal–Metal Interactions. II. Accelerating Generalized Schemes through Physical Insights. *J. Chem. Phys.* **2020**, *152*, 094702.
- (41) Ding, Y.; Xu, Y.; Mao, Y.; Wang, Z.; Hu, P. Achieving Rational Design of Alloy Catalysts Using a Descriptor Based on a Quantitative Structure–Energy Equation. *Chem. Commun.* **2020**, *56*, 3214–3217.
- (42) Aarons, J.; Jones, L.; Varambhia, A.; MacArthur, K. E.; Ozkaya, D.; Sarwar, M.; Skylaris, C.-K.; Nellist, P. D. Predicting the Oxygen-Binding Properties of Platinum Nanoparticle Ensembles by Combining High-Precision Electron Microscopy and Density Functional Theory. *Nano Lett.* **2017**, *17*, 4003–4012.
- (43) Tripković, V.; Cerri, I.; Bligaard, T.; Rossmeisl, J. The Influence of Particle Shape and Size on the Activity of Platinum Nanoparticles for Oxygen Reduction Reaction: A Density Functional Theory Study. *Catal. Lett.* **2014**, *144*, 380–388.
- (44) Rossi, K.; Asara, G. G.; Baletto, F. Structural Screening and Design of Platinum Nanosamples for Oxygen Reduction. *ACS Catal.* **2020**, *10*, 3911–3920.
- (45) Rück, M.; Bandarenka, A.; Calle-Vallejo, F.; Gagliardi, A. Oxygen Reduction Reaction: Rapid Prediction of Mass Activity of Nanostructured Platinum Electrocatalysts. *J. Phys. Chem. Lett.* **2018**, *9*, 4463–4468.
- (46) Chattaraj, P. K.; Maiti, B.; Sarkar, U. Philicity: A Unified Treatment of Chemical Reactivity and Selectivity. *J. Phys. Chem. A* **2003**, *107*, 4973–4975.
- (47) Ayers, P. W.; Anderson, J. S. M.; Bartolotti, L. J. Perturbative Perspectives on the Chemical Reaction Prediction Problem. *Int. J. Quantum Chem.* **2005**, *101*, 520–534.
- (48) Jiao, S.; Fu, X.; Huang, H. Descriptors for the Evaluation of Electrocatalytic Reactions: d-Band Theory and Beyond. *Adv. Funct. Mater.* **2022**, *32*, 2107651.
- (49) Vojvodic, A.; Nørskov, J. K.; Abild-Pedersen, F. Electronic Structure Effects in Transition Metal Surface Chemistry. *Top. Catal.* **2014**, *57*, 25–32.
- (50) Saini, S.; Stenlid, J. H.; Abild-Pedersen, F. Electronic Structure Factors and the Importance of Adsorbate Effects in Chemisorption on Surface Alloys. *npj Comput. Mater.* **2022**, *8*, 1–12.
- (51) Stenlid, J. H.; Streibel, V.; Choksi, T. S.; Abild-Pedersen, F. Assessing Catalytic Rates of Bimetallic Nanoparticles with Active-Site Specificity: A Case Study Using NO Decomposition. *Chem Catalysis* **2023**, *3*, 100636.
- (52) Jørgensen, M.; Grönbeck, H. Perspectives on Computational Catalysis for Metal Nanoparticles. *ACS Catal.* **2019**, *9*, 8872–8881.
- (53) Brinck, T.; Stenlid, J. H. The Molecular Surface Property Approach: A Guide to Chemical Interactions in Chemistry, Medicine, and Material Science. *Advanc. Theo. Catal.* **2019**, *2*, 1800149.
- (54) Frontera, A.; Bauzá, A. Regium– π Bonds: An Unexplored Link between Noble Metal Nanoparticles and Aromatic Surfaces. *Chemistry – A European Journal* **2018**, *24*, 7228–7234.

- (55) Stenlid, J. H.; Brinck, T. Extending the σ -Hole Concept to Metals: An Electrostatic Interpretation of the Effects of Nanostructure in Gold and Platinum Catalysis. *J. Am. Chem. Soc.* **2017**, *139*, 11012–11015.
- (56) Stenlid, J. H.; Johannes Johansson, A.; Brinck, T. The Local Electron Attachment Energy and the Electrostatic Potential as Descriptors of Surface–Adsorbate Interactions. *Phys. Chem. Chem. Phys.* **2019**, *21*, 17001–17009.
- (57) Stenlid, J. H.; Johansson, A. J.; Brinck, T. σ -Holes on Transition Metal Nanoclusters and Their Influence on the Local Lewis Acidity. *Crystals* **2017**, *7*, 222.
- (58) Stenlid, J. H.; Johansson, A. J.; Brinck, T. σ -Holes and σ -Lumps Direct the Lewis Basic and Acidic Interactions of Noble Metal Nanoparticles: Introducing Regium Bonds. *Phys. Chem. Chem. Phys.* **2018**, *20*, 2676–2692.
- (59) Stenlid, J. H.; Johansson, A. J.; Brinck, T. Local Lewis Acidity of $(\text{TiO}_2)_n$ $N=7$ -10 Nanoparticles Characterized by DFT-Based Descriptors: Tools for Catalyst Design. *J. Phys. Chem. C* **2017**, *121*, 27483–27492.
- (60) Stenlid, J. H.; Brinck, T. Nucleophilic Aromatic Substitution Reactions Described by the Local Electron Attachment Energy. *J. Org. Chem.* **2017**, *82*, 3072–3083.
- (61) Li, G.; Stenlid, J. H.; Ahlquist, M. S. G.; Brinck, T. Utilizing the Surface Electrostatic Potential to Predict the Interactions of Pt and Ni Nanoparticles with Lewis Acids and Bases— σ -Lumps and σ -Holes Govern the Catalytic Activities. *J. Phys. Chem. C* **2020**, *124*, 14696–14705.
- (62) Brinck, T.; Carlqvist, P.; Stenlid, J. H. Local Electron Attachment Energy and Its Use for Predicting Nucleophilic Reactions and Halogen Bonding. *J. Phys. Chem. A* **2016**, *120*, 10023–10032.
- (63) Stenlid, J. H.; Campos dos Santos, E.; Johansson, A. J.; Pettersson, L. G. M. On the Nature of the Cathodic Reaction during Corrosion of Copper in Anoxic Sulfide Solutions. *J. Electrochem. Soc.* **2019**, *166*, C196–C208.
- (64) Suresh, C. H.; Remya, G. S.; Anjalikrishna, P. K. Molecular Electrostatic Potential Analysis: A Powerful Tool to Interpret and Predict Chemical Reactivity. *Wiley Interdiscip. Rev. Comput. Mol. Sci.* **2022**, *12*, e1601.
- (65) Murray, J. S.; Politzer, P. The Electrostatic Potential: An Overview. *Wiley Interdiscip. Rev. Comput. Mol. Sci.* **2011**, *1*, 153–163.
- (66) Lohr, L. L. Protonic Counterpart of Electronegativity as an Organizing Principle for Acidity and Basicity. *J. Phys. Chem.* **1984**, *88*, 3607–3611.
- (67) Lohr, L. L. The Protonic Counterpart of Electronegativity. *Int. J. Quantum Chem.* **1985**, *28*, 731–732.
- (68) Ayers, P. W. Variational Principles for Describing Chemical Reactions, University of North Carolina, Chapel Hill, 2001.
- (69) Politzer, P.; Murray, J. S. Electrostatic Potentials at the Nuclei of Atoms and Molecules. *Theor. Chem. Acc.* **2021**, *140*, 7.
- (70) Sheppard, D.; Henkelman, G.; von Lilienfeld, O. A. Alchemical Derivatives of Reaction Energetics. *J. Chem. Phys.* **2010**, *133*, 084104.
- (71) Saravanan, K.; Kitchin, J. R.; von Lilienfeld, O. A.; Keith, J. A. Alchemical Predictions for Computational Catalysis: Potential and Limitations. *J. Phys. Chem. Lett.* **2017**, *8*, 5002–5007.
- (72) Griego, C. D.; Maldonado, A. M.; Zhao, L.; Zulueta, B.; Gentry, B. M.; Lipsman, E.; Choi, T. H.; Keith, J. A. Computationally Guided Searches for Efficient Catalysts through Chemical/Materials Space: Progress and Outlook. *J. Phys. Chem. C* **2021**, *125*, 6495–6507.
- (73) Kaya, S.; Robles-Navarro, A.; Mejía, E.; Gómez, T.; Cardenas, C. On the Prediction of Lattice Energy with the Fukui Potential: Some Supports on Hardness Maximization in Inorganic Solids. *J. Phys. Chem. A* **2022**, *126*, 4507–4516.

- (74) Gómez, T.; Fuentealba, P.; Robles-Navarro, A.; Cárdenas, C. Links among the Fukui Potential, the Alchemical Hardness and the Local Hardness of an Atom in a Molecule. *J. Comput. Chem.* **2021**, *42*, 1681–1688.
- (75) Cerón, M. L.; Gomez, T.; Calatayud, M.; Cárdenas, C. Computing the Fukui Function in Solid-State Chemistry: Application to Alkaline Earth Oxides Bulk and Surfaces. *J. Phys. Chem. A* **2020**, *124*, 2826–2833.
- (76) Muñoz, M.; Cárdenas, C. How Predictive Could Alchemical Derivatives Be? *Phys. Chem. Chem. Phys.* **2017**, *19*, 16003–16012.
- (77) Cárdenas, C.; Tiznado, W.; Ayers, P. W.; Fuentealba, P. The Fukui Potential and the Capacity of Charge and the Global Hardness of Atoms. *J. Phys. Chem. A* **2011**, *115*, 2325–2331.
- (78) Cohen, M. H.; Ganduglia-Pirovano, M. V.; Kudrnovský, J. Reactivity Kernels, the Normal Modes of Chemical Reactivity, and the Hardness and Softness Spectra. *J. Chem. Phys.* **1995**, *103*, 3543–3551.
- (79) Cohen, M. H.; Ganduglia-Pirovano, M. V.; Natoli, V.; Kudrnovsky, J. Chemical Reactivity Theory for Physicists; a Work in Progress. *ChemInform* **1996**, *27*, 315–333. *Quantum Theory Real Mater.*, **1996**, 315-333.
- (80) Cohen, M. H.; Ganduglia-Pirovano, M. V.; Kudrnovský, J. Electronic and Nuclear Chemical Reactivity. *J. Chem. Phys.* **1994**, *101*, 8988–8997.
- (81) Aliaga, C.; Fuentealba, P.; Muñoz, F.; Pastenes, C.; Rezende, M. C.; Spodine, E.; Cárdenas, C. Interaction of Nitroxide Radicals with an Au₈ Nanostructure: Theoretical and Calorimetric Studies. *J. Phys. Chem. C* **2019**, *123*, 21713–21720.
- (82) Cardenas, C.; Munoz, M. M.; Contreras, J.; Ayers, P. W.; Gomez, T.; Fuentealba, P. Understanding Chemical Reactivity in Extended Systems: Exploring Models of Chemical Softness in Carbon Nanotubes. *Acta Phys.-Chim. Sin.* **2018**, *34*, 631–638.
- (83) Muñoz, M.; Robles-Navarro, A.; Fuentealba, P.; Cárdenas, C. Predicting Deprotonation Sites Using Alchemical Derivatives. *J. Phys. Chem. A* **2020**, *124*, 3754–3760.
- (84) Anjali, B. A.; Sayyed, F. B.; Suresh, C. H. Correlation and Prediction of Redox Potentials of Hydrogen Evolution Mononuclear Cobalt Catalysts via Molecular Electrostatic Potential: A DFT Study. *J. Phys. Chem. A* **2016**, *120*, 1112–1119.
- (85) Politzer, P.; Murray, J. S. The Fundamental Nature and Role of the Electrostatic Potential in Atoms and Molecules. *Theor. Chem. Acc.* **2002**, *108*, 134–142.
- (86) Politzer, P.; Parr, R. G. Some New Energy Formulas for Atoms and Molecules. *J. Chem. Phys.* **1974**, *61*, 4258–4262.
- (87) Politzer, P.; Murray, J. S. The Neglected Nuclei. *Molecules* **2021**, *26*, 2982.
- (88) Capitani, J. F.; Nalewajski, R. F.; Parr, R. G. Non-Born–Oppenheimer Density Functional Theory of Molecular Systems. *J. Chem. Phys.* **1982**, *76*, 568–573.
- (89) Nalewajski, R. F.; Capitani, J. F. Density Functional Theory: Non-Born–Oppenheimer Legendre Transforms and Maxwell Relations, Equilibrium and Stability Conditions. *J. Chem. Phys.* **1982**, *77*, 2514–2526.
- (90) Kresse, G.; Furthmüller, J. Efficient Iterative Schemes for Ab Initio Total-Energy Calculations Using a Plane-Wave Basis Set. *Phys. Rev. B* **1996**, *54*, 11169–11186.
- (91) Kresse, G.; Hafner, J. Ab Initio Molecular Dynamics for Liquid Metals. *Phys. Rev. B* **1993**, *47*, 558–561.
- (92) Hammer, B.; Hansen, L. B.; Nørskov, J. K. Improved Adsorption Energetics within Density-Functional Theory Using Revised Perdew-Burke-Ernzerhof Functionals. *Phys. Rev. B* **1999**, *59*, 7413–7421.
- (93) Blöchl, P. E. Projector Augmented-Wave Method. *Phys. Rev. B* **1994**, *50*, 17953–17979.
- (94) Kresse, G.; Joubert, D. From Ultrasoft Pseudopotentials to the Projector Augmented-Wave Method. *Phys. Rev. B* **1999**, *59*, 1758–1775.

- (95) Larsen, A. H.; Mortensen, J. J.; Blomqvist, J.; Castelli, I. E.; Christensen, R.; Dulak, M.; Friis, J.; Groves, M. N.; Hammer, B.; Hargus, C.; et al. The Atomic Simulation Environment—a Python Library for Working with Atoms. *J. Phys.: Condens. Matter* **2017**, *29*, 273002.
- (96) Wang, V.; Xu, N.; Liu, J.-C.; Tang, G.; Geng, W.-T.; VASPKIT: A User-Friendly Interface Facilitating High-Throughput Computing and Analysis Using VASP Code. *Comput. Phys. Commun.* **2021**, *267*, 108033.
- (97) Momma, K.; Izumi, F. VESTA 3 for Three-Dimensional Visualization of Crystal, Volumetric and Morphology Data., *J. Appl. Crystallogr.* **2011**, *44*, 1272–1276.
- (98) Bader, R. F. W. *Atoms in Molecules - A Quantum Theory*; Oxford University Press, 1990.
- (99) Winther, K. T.; Hoffmann, M. J.; Boes, J. R.; Mamun, O.; Bajdich, M.; Bligaard, T. Catalysis-Hub.Org, an Open Electronic Structure Database for Surface Reactions. *Sci. Data.* **2019**, *6*, 75.
- (100) Roling, L. T.; Abild-Pedersen, F. Structure-Sensitive Scaling Relations: Adsorption Energies from Surface Site Stability. *ChemCatChem* **2018**, *10*, 1643–1650.
- (101) Clark, T.; Hennemann, M.; Murray, J.; Politzer, P. Halogen Bonding: The σ -Hole. *J. Mol. Model.* **2007**, *13*, 291–296.
- (102) Politzer, P.; Murray, J. S.; Clark, T. Halogen Bonding: An Electrostatically-Driven Highly Directional Noncovalent Interaction. *Phys. Chem. Chem. Phys.* **2010**, *12*, 7748–7757.
- (103) Brinck, T.; Murray, J. S.; Politzer, P. Surface Electrostatic Potentials of Halogenated Methanes as Indicators of Directional Intermolecular Interactions. *Int. J. Quantum Chem.* **1992**, *44*, 57–64.
- (104) Bultinck, P.; Cardenas, C.; Fuentealba, P.; Johnson, P. A.; Ayers, P. W. Atomic Charges and the Electrostatic Potential Are Ill-Defined in Degenerate Ground States. *J. Chem. Theory Comput.* **2013**, *9*, 4779–4788.
- (105) Cárdenas, C.; Ayers, P. W.; Cedillo, A. Reactivity Indicators for Degenerate States in the Density-Functional Theoretic Chemical Reactivity Theory. *J. Chem. Phys.* **2011**, *134*, 174103.
- (106) Omrani, M.; Goriaux, M.; Liu, Y.; Martinet, S.; Jean-Soro, L.; Ruban, V. Platinum Group Elements Study in Automobile Catalysts and Exhaust Gas Samples. *Environ. Pollut.* **2020**, *257*, 113477.
- (107) Farrauto, R. J.; Heck, R. M. Catalytic Converters: State of the Art and Perspectives. *Catal. Today* **1999**, *51* (3), 351–360.
- (108) Piotrowski, M. J.; Piquini, P.; Da Silva, J. L. F. Density Functional Theory Investigation of 3d, 4d, and 5d 13-Atom Metal Clusters. *Phys. Rev. B* **2010**, *81*, 155446.
- (109) Sun, G.; Sautet, P. Active Site Fluxional Restructuring as a New Paradigm in Triggering Reaction Activity for Nanocluster Catalysis. *Acc. Chem. Res.* **2021**, *54*, 3841–3849.
- (110) Zhang, Z.; Zandkarimi, B.; Munarriz, J.; Dickerson, C. E.; Alexandrova, A. N. Fluxionality of Subnano Clusters Reshapes the Activity Volcano of Electrocatalysis. *ChemCatChem* **2022**, *14*, e202200345.
- (111) Fung, V.; Jiang, D. Exploring Structural Diversity and Fluxionality of Pt_n (n = 10–13) Clusters from First-Principles. *J. Phys. Chem. C* **2017**, *121*, 10796–10802.
- (112) Zandkarimi, B.; Alexandrova, A. N. Dynamics of Subnanometer Pt Clusters Can Break the Scaling Relationships in Catalysis. *J. Phys. Chem. Lett.* **2019**, *10*, 460–467.
- (113) Zhai, H.; Alexandrova, A. N. Fluxionality of Catalytic Clusters: When It Matters and How to Address It. *ACS Catal.* **2017**, *7*, 1905–1911.
- (114) Jiang, D.; Wan, G.; Stenlid, J.H.; García-Vargas, C. E.; Zhang, J.; Sun, C.; Li, J.; Abild-Pedersen, F.; Tassone, C. J.; Wang, Y. Dynamic and Reversible Transformations of Subnanometre-Sized Palladium on Ceria for Efficient Methane Removal. *Nat. Catal.* **2023**, 1–10.
- (115) Lamoureux, P. S.; Choksi, T. S.; Streibel, V.; Abild-Pedersen, F. Combining Artificial Intelligence and Physics-Based Modeling to Directly Assess Atomic Site Stabilities: From Sub-Nanometer Clusters to Extended Surfaces. *Phys. Chem. Chem. Phys.* **2021**, *23*, 22022–22034.

- (116) Campbell, C. T. The Energetics of Supported Metal Nanoparticles: Relationships to Sintering Rates and Catalytic Activity. *Acc. Chem. Res.* **2013**, *46*, 1712–1719.
- (117) Mao, Z.; Campbell, C. T. Predicting a Key Catalyst-Performance Descriptor for Supported Metal Nanoparticles: Metal Chemical Potential. *ACS Catal.* **2021**, *11*, 8284–8291.
- (118) Wilson, E. B. Four-Dimensional Electron Density Function. *J. Chem. Phys.* **1962**, *36*, 2232–2233.
- (119) Gauthier, J. A.; Stenlid, J. H.; Abild-Pedersen, F.; Head-Gordon, M.; Bell, A. T. The Role of Roughening to Enhance Selectivity to C₂₊ Products during CO₂ Electroreduction on Copper. *ACS Energy Lett.* **2021**, *6*, 3252–3260.
- (120) Zamora Zeledón, J. A.; Stevens, M. B.; Gunasooriya, G. T. K. K.; Gallo, A.; Landers, A. T.; Kreider, M. E.; Hahn, C.; Nørskov, J. K.; Jaramillo, T. F. Tuning the Electronic Structure of Ag-Pd Alloys to Enhance Performance for Alkaline Oxygen Reduction. *Nat. Commun.* **2021**, *12*, 620.
- (121) Dasgupta, A.; He, H.; Gong, R.; Shang, S.-L.; Zimmerer, E. K.; Meyer, R. J.; Liu, Z.-K.; Janik, M. J.; Rioux, R. M. Atomic Control of Active-Site Ensembles in Ordered Alloys to Enhance Hydrogenation Selectivity. *Nat. Chem.* **2022**, *14*, 523–529.
- (122) Xin, H.; Linic, S. Communications: Exceptions to the d-Band Model of Chemisorption on Metal Surfaces: The Dominant Role of Repulsion between Adsorbate States and Metal d-States. *J. Chem. Phys.* **2010**, *132*, 221101.
- (123) Grabow, L. C.; Hvolbæk, B.; Nørskov, J. K. Understanding Trends in Catalytic Activity: The Effect of Adsorbate–Adsorbate Interactions for CO Oxidation Over Transition Metals. *Top. Catal.* **2010**, *53*, 298–310.
- (124) Skúlason, E.; Jónsson, H. Atomic Scale Simulations of Heterogeneous Electrocatalysis: Recent Advances. *Adv. Phys. X* **2017**, *2*, 481–495.